

Measuring Top Yukawa Coupling through $2 \rightarrow 3$ VBS at Muon Collider

Junmou Chen,^{1,*} Junhong Chen,^{1,†} and Wei He^{1,‡}

¹*Jinan University, Guangzhou, Guangdong, China*

Abstract

We study the measurement of top Yukawa coupling through $2 \rightarrow 3$ VBS at future muon colliders, focusing on the lepton and semi-lepton channels of $\nu\bar{\nu}t\bar{t}h/z$. First, analyzing the partonic amplitudes of $W_L W_L \rightarrow t\bar{t}h/Z_L$ and simulating the full processes of $\nu\bar{\nu}t\bar{t}h/z$ without decaying, we find they are highly sensitive to the anomalous top Yukawa δy_t . This sensitivity is enhanced by selecting helicities of the final $t\bar{t}$ and Z to be $t_L\bar{t}_L + t_R\bar{t}_R$ and Z_L , which serves as the default and core setting of our analysis. We then obtain the limits on δy_t with this setting, giving $[-1.0\%, 1.1\%]$ for $\nu\bar{\nu}t\bar{t}h$ only and $[-0.36\%, 0.92\%]$ for $\nu\bar{\nu}t\bar{t}h$ and $\nu\bar{\nu}t\bar{t}z$ combined at 30 TeV and 1σ . Second, we proceed to analyze the processes after decaying and with background processes. To enhance the sensitivity to δy_t , our settings include selecting the helicities of the final particles, as well as applying suitable cuts. However, we don't do bin-by-bin analysis. We obtain the limits on δy_t for those channels at 10/30 TeV and $1\sigma/2\sigma$. The best limit is from the semi-lepton channel of $\nu\bar{\nu}t\bar{t}h$. With spin tagging efficiency at $\epsilon_s = 0.9$, it gives $[-1.6\%, 1.8\%]$ at 1σ and $[-2.4\%, 2.7\%]$ at 2σ at 30 TeV; $[-7.0\%, 6.7\%]$ at 1σ and $[-9.8\%, 9.8\%]$ at 2σ at 10 TeV.

* chenjm@jnu.edu.cn

† 2aron@stu2021@jnu.edu.cn

‡ weii20021121@stu2021.jnu.edu.cn

I. INTRODUCTION

The top Yukawa coupling is one of the most important parameters in the standard model(SM), probably second only to Higgs self-couplings. In many new physics models, it's closely related to solution of the hierarchy problem, see for example[1–3]. Moreover, the CP phase of top Yukawa could be related to the matter-anti-matter asymmetry of our universe[4, 5]. Thus a precise measurement of top Yukawa is of great importance in the research of particle physics today. This importance is further enhanced in light of the null result of discovering supersymmetric particles or new particles in other new physics models[6–8] at LHC.

Currently in LHC the top Yukawa coupling and its CP phase have been measured through tth and th channels[9–11], albeit with large uncertainties. For example, the uncertainty of top Yukawa is still around 50% at 2σ ([11]). This is to be expected, since hadron colliders are not designed for precision measurement due to its messy background. Therefore, it's important to consider other options such as new colliders, among which muon collider is a particularly attractive candidate because of its advantages of both clean background and high energy. Because of this advantage, future high energy muon collider has received considerable interests in the literature in recent years[12–17]. As for top Yukawa measurement in muon collider, most research in the literature so far focuses on the νtt channel, including for the top Yukawa coupling in [18–22] and its CP phase in [23], which has the largest cross section for top production. In [22], the authors found δy_t can be constrained up to 1.5%(1σ) at 10 TeV muon collider with 10 ab^{-1} luminosity, while in [21] the precision of y_t at 2σ is projected to be 4.5%(1.4%) at 10 TeV(30 TeV). Besides νtt , there are also a few studies on other channels, see [24] and [21]. In the former, νtth and $lvtbh$ are studied along with νtt in measuring the CP phase. In the latter, the measurement of top Yukawa is studied using νtth , along with νtt as mentioned above. The limits on δy_t at 2σ level from νtth were obtained to be around 5.5%(0.69%) at 10(30) TeV. In both cases cited above([21, 22]), the analysis is done with the final states($\nu tt/\nu tth$) directly without decaying and hadronization, with no or only superficial background analysis. Moreover, they both use bin-by-bin method in data analysis. Thus their results are highly idealized.

The focus on the νtt channel is understandable, considering its large cross section. However, it's also important to consider and further explore other options. In this paper, we

study the potential of using $2 \rightarrow 3$ vector boson scattering(VBS) processes ($VV \rightarrow t\bar{t}h/V_L$) to measure the top Yukawa coupling, including but not limited to the $\nu\nu t\bar{t}h$ channel. The motivation can be simply explained in the following. By taking Goldstone equivalence, the $2 \rightarrow 3$ VBS amplitude with longitudinal vector bosons has a contact diagram from a dim-6 SMEFT operator (\mathcal{O}_6 in the case of $\varphi\varphi \rightarrow \varphi\varphi h(V_L V_L \rightarrow V_L V_L h)$, $\mathcal{O}_{t\Phi}$ ([25]) in the case of $\varphi\varphi \rightarrow t\bar{t}h/\varphi(V_L V_L \rightarrow t\bar{t}h/V_L)$). In high energy, the contact diagram dominates the amplitude. Since $\mathcal{O}_{t\Phi}$ — the SMEFT operator that gives the contact diagram — also gives rise to an anomalous top Yukawa coupling δy_t , we conclude that the VBS process would be highly sensitive to δy_t . This situation is in analogue to the measurement of Higgs self-couplings through $\nu\nu V_L V_L h$ channels as done in [26, 27]. Crucially, the above analysis would lead to the conclusion that the helicities of final $t\bar{t}$ have to be $t_R\bar{t}_R$ or $t_L\bar{t}_L$ in high energy. The analysis will be explained in more details in the next section.

In this paper we won't touch on the top CP phase, but focus on the anomalous top Yukawa coupling δy_t only. There are two goals of our paper: First we intend to find a simple method to achieve high significance, which do not rely on bin-by-bin analysis used in [26, 27] and etc. Since it is very time consuming and more appropriate for optimization after a simple method has been found to achieve high sensitivity. Second, we wish to obtain more reliable estimations for δy_t . Our central setting to achieve the first goal is to select helicities of final states ($t\bar{t}$ and V before decaying) to be $t_R\bar{t}_R + t_L\bar{t}_L$ and V_L . For the second goal, we will carry out a more complete analysis by decaying the final states $t\bar{t}$ and h/V and simulating background processes along with the signal. We then analyze the data with the combination of selecting final states' helicities and some simple cuts. Finally we choose to do the analysis at the center-of-mass energy(c.m.) of $\sqrt{s} = 10, 30$ TeV.

The rest of the paper is organized as following:

In Section (II), we will study the processes at the level of the VBS processes and hard processes before decaying. Focusing on $\nu\nu t\bar{t}h/z$ after listing all $2 \rightarrow 3$ VBS related to top production, we first analyse the amplitude of $W_L W_L \rightarrow t\bar{t}h/Z_L$ with $\mathcal{O}_{t\Phi}$. After that, we obtain the statistic significance of $\nu\nu t\bar{t}h/z$ with and without selecting helicities as comparison, within a range of c.m. energies. We finally obtain the limit of δy_t for $\nu\nu t\bar{t}h/z$ without decaying and background analysis, as an approximation to the limits of all the data when made use of sufficiently.

In Section (III), we study $\nu\nu t\bar{t}h$ at the lepton channel and the semi-lepton channel re-

spectively. We generate all important background processes, then obtain the cuts to reduce the background relative to signal. We then obtain the limits on $\delta y_t(c_{t\phi})$ at 30 TeV and 10 TeV, unless the statistical significance is too small.

In Section (IV), we study $\nu\bar{\nu}ttz$ at the lepton channel and the semi-lepton channel, following the same approach in Sec.(III).

In Conclusion (V), we summary and discuss our results, compare them with the literature, and finally discuss future research directions.

II. FIRST ANALYSIS OF PARTON AND HARD PROCESSES

A. Partonic Processes: $VV \rightarrow t\bar{t}V/h$

In high energy muon colliders, vector boson scatterings become the dominant channels in producing top quarks. For $2 \rightarrow 3$ VBS we have the following list of processes that are sensitive to the anomalous top Yukawa coupling:

$$W^+W^-/ZZ \rightarrow t\bar{t}h, \quad W^+W^-/ZZ \rightarrow t\bar{t}Z, \quad W^+W^-/ZZ \rightarrow t\bar{b}W^- (/t\bar{b}W^+) \quad (1)$$

$$W^\pm Z \rightarrow t\bar{t}W^\pm, \quad W^\pm Z \rightarrow t\bar{b} (/b\bar{t})Z, \quad (2)$$

WW scatterings correspond to $\mu\mu \rightarrow \nu\bar{\nu}X$ in a muon collider, ZZ scatterings correspond to $\mu\mu \rightarrow \mu\mu X$, while WZ scatterings correspond to $\mu\mu \rightarrow \mu\nu X$. In this paper we focus on WW scatterings only, since in our experience their cross sections dominate over the others. Moreover, $W^+W^-/ZZ \rightarrow t\bar{b}W^- (/t\bar{b}W^+)$ has the same final states as $WW \rightarrow t\bar{t}, t/\bar{t} \rightarrow bW$, thus should be analyzed together with $2 \rightarrow 2$ VBS. So it won't be part of our study here either. Therefore the processes we study in this paper are

$$W^+W^- \rightarrow t\bar{t}h, \quad W^+W^- \rightarrow t\bar{t}Z, \quad (3)$$

The general Lagrangian terms that give the top Yukawa coupling can be written as following:

$$\mathcal{L} \supset -\frac{y_t^{\text{SM}}}{\sqrt{2}} \kappa_t \bar{t} (\cos \delta + i\gamma_5 \sin \delta) t h \quad (4)$$

$y_t^{\text{SM}} = \sqrt{2}m_t/v$ is the SM value of top Yukawa, κ_t and CP phase δ are free parameters that measure the deviation from the SM. In this paper we're not interested in CP violation, so δ

is set to be 0 from now on. We further split κ_t as $\kappa_t = 1 + \delta y_t$, the Lagrangian then becomes

$$\mathcal{L} \supset -\frac{y_t^{\text{SM}}}{\sqrt{2}}(1 + \delta y_t)\bar{t}th \quad (5)$$

However, Eq.(4) and Eq.(5) do not include all relevant physics, since the Higgs boson in the SM belongs to a $SU(2)$ doublet, along with other would-be Goldstone bosons φ^\pm, φ^0 . To include them, we need to consider the gauge invariant SM Lagrangian:

$$\mathcal{L} \supset -y_t^{\text{SM}}\bar{Q}t_R\tilde{\Phi} + \text{h.c.} \quad (6)$$

in which $Q = (t_L, b_L)^T$, $\Phi = (\varphi^+, \frac{1}{\sqrt{2}}(h + i\varphi^0))^T$ and $\tilde{\Phi}_a = \epsilon_{ab}\Phi_b$. To further accommodate the anomalous top Yukawa coupling gauge invariantly, we can add the SMEFT operator

$$\mathcal{O}_{t\phi} = \frac{c_{t\phi}}{\Lambda^2}\bar{Q}t_R\tilde{\Phi}(\Phi^\dagger\Phi) + \text{h.c.} \quad (7)$$

The energy scale Λ is taken to be 1 TeV in this paper, we can also define $C_{t\phi} \equiv \frac{c_{t\phi}}{\Lambda^2}$ to absorb Λ into $c_{t\phi}$.

In unitarity gauge, Eq.(6) and Eq.(7) combined gives the tth coupling in Eq.(4) with

$$\Delta y_t \equiv \delta y_t \cdot y_t^{\text{SM}} = -\frac{c_{t\phi}v^2}{\Lambda^2}. \quad (8)$$

Although in principle all physical information can be extracted in unitary gauge, it's usually not the most convenient and physically clarifying approach, because of the large cancellation between Feynman diagrams. Instead, we choose a gauge with Goldstone bosons (e.g. Feynman gauge) and take Goldstone equivalence, which simplify the analysis significantly.

Let's analyze the amplitude of $W_L^+W_L^- \rightarrow t\bar{t}h$ as an example, which can be approximated by $\varphi^+\varphi^- \rightarrow t\bar{t}h$ in high energy. Notice $\mathcal{O}_{t\phi}$ (Eq.(7)) gives a 5-point contact vertex/diagram: $\lambda_{\varphi\phi tth} = i\frac{c_{t\phi}v^2}{\sqrt{2}\Lambda^2}$. In the high energy limit, other diagrams with one or two propagators are suppressed by $\mathcal{O}(\frac{1}{E^2})$, while only the contact diagram remains constant¹. The BSM amplitude with $\lambda_{\varphi\phi tth}$ is therefore approximately:

$$\mathcal{A}_{\text{BSM}} \simeq i\frac{c_{t\phi}v^2}{\sqrt{2}\Lambda^2} + \mathcal{O}(\frac{m_W^2}{E^2}). \quad (9)$$

In contrast, the SM amplitude is suppressed by energy:

$$\mathcal{A}_{\text{SM}} \simeq \mathcal{O}(\frac{m_W^2}{E^2}). \quad (10)$$

¹ Soft/collinear logarithm can elevate this suppression to certain extent, but don't change the qualitative picture.

Comparing BSM and SM amplitudes indicates high sensitivity of $\nu vtth$ to δy_t , giving justification for our choice of processes in this paper. The similar conclusion can be drawn for $WW \rightarrow t\bar{t}Z$. Of course, in order for Goldstone equivalence to apply, Z has to be longitudinal so that $Z_L \sim \phi^0$ in high energy.

There remains a subtlety with the analysis above, involving the helicities of $t\bar{t}$. Notice $\mathcal{O}_{t\phi}$ gives the chiral structure of $\bar{t}_L t_R$ or $\bar{t}_R t_L$, similar to the SM tth coupling. In high energy limit for the final states, $t_{L/R}$ in chirality corresponds to $t_{L/R}$ in helicity only, while $\bar{t}_{L/R}$ in chirality corresponds to $\bar{t}_{R/L}$ in helicity only. Therefore, only $\bar{t}_R t_R$ or $\bar{t}_L t_L$ (in helicity) contributes to the contact diagram $\lambda_{\varphi^+\varphi^-tth}(\lambda_{\varphi^+\varphi^-tt\varphi^0})$ of $\varphi^+\varphi^- \rightarrow t\bar{t}h(\varphi^+\varphi^- \rightarrow t\bar{t}\varphi^0)$.

The finding above indicates we can significantly enhance the sensitivity to the anomalous top Yukawa by selecting the helicities of the final $t\bar{t}$ and Z . We can make a rough estimation of the enhancement to statistical significance, as defined by

$$Z \simeq \frac{S}{\sqrt{B}} = \frac{\sqrt{\mathcal{L}} \cdot \sigma^{\text{sig}}}{\sqrt{\sigma^{\text{bkg}}}} \quad (11)$$

with S and B being event numbers of signal and background respectively, \mathcal{L} being integrated luminosity. For $\nu vtth$, the ratio of the cross section of summing over all spins to that of $t_L \bar{t}_L + t_R \bar{t}_R$ is roughly 2 : 1; while for νvtz , the ratio of full cross section to that of $t_L \bar{t}_L Z_L + t_R \bar{t}_R Z_L$ is around 5 : 1. Then the ratio of statistic significance from selecting helicity to not selecting helicity is

$$\begin{aligned} \nu vtth : \quad \frac{Z_{\text{spin}}}{Z_{\text{no-spin}}} &= \sqrt{\frac{\sigma_{\text{no-spin}}^{\text{bkg}}}{\sigma_{\text{spin}}^{\text{bkg}}}} = \sqrt{2} \simeq 1.4 \\ \nu vtz : \quad \frac{Z_{\text{spin}}}{Z_{\text{no-spin}}} &= \sqrt{5} \simeq 2.23, \end{aligned} \quad (12)$$

giving 40% enhancement for $\nu vtth$ and 120% enhancement for νvtz . Notice the dependence on σ^{sig} and \mathcal{L} cancels out.

B. Sensitivity of $\nu vtth/\nu vtz$ to $\delta y_t(c_{t\phi})$

To have more accurate and general estimations, we use Madgraph5[28](version 3.4.1) to generate the total cross sections of $\nu vtth$ and νvtz with different helicity combinations, and without decaying or considering background processes. The BSM processes are generated with SMEFTatNLO([29]) package at LO mode, $c_{t\phi}$ is set at $c_{t\phi} = 2$ and $\Lambda = 1$ TeV. The

c.m energy is scanned from 10 TeV to 30 TeV. For the statistical significance we use the following formula:

$$Z = \sqrt{2 \left[(S + B) \cdot \ln \left(1 + \frac{S}{B} \right) - S \right]} \quad (13)$$

The signal ‘‘S’’ is

$$S = (\sigma_{\text{bsm}}^{\text{sig}} - \sigma_{\text{sm}}^{\text{sig}}) \cdot \mathcal{L} \quad (14)$$

the background ‘‘B’’ is

$$B = \sigma^{\text{bkg}} \cdot \mathcal{L}. \quad (15)$$

Here ‘‘sig’’ signifies the processes $\mu\mu \rightarrow \nu\bar{\nu}t_R\bar{t}_R(/t_L\bar{t}_L)h$ and/or $\mu\mu \rightarrow \nu\bar{\nu}t_R\bar{t}_R(/t_L\bar{t}_L)Z_L$, ‘‘bkg’’ signifies all other processes involved.

We obtain the integrated luminosity by using the following formula

$$\mathcal{L} = \left(\frac{\sqrt{s}}{10 \text{ TeV}} \right)^2 \cdot 10 \text{ ab}^{-1} \quad (16)$$

which for example gives 10, 90 ab^{-1} for $\sqrt{s} = 10, 30$ TeV respectively.

The results are shown in Fig.(1) for $\nu\bar{\nu}t\bar{t}h$ and Fig.(2) for $\nu\bar{\nu}t\bar{t}z$. In Fig.(1), we show the cross sections and significance of $\nu\bar{\nu}t_R\bar{t}_Rh + \nu\bar{\nu}t_L\bar{t}_Lh$, $\nu\bar{\nu}t_R\bar{t}_Lh + \nu\bar{\nu}t_L\bar{t}_Rh$ and $\nu\bar{\nu}t\bar{t}h$ without selecting helicities of $t\bar{t}$. In Fig.(2), we show the cross sections and significance of $\nu\bar{\nu}t_R\bar{t}_RZ_L + \nu\bar{\nu}t_L\bar{t}_LZ_L$, $\nu\bar{\nu}t_R\bar{t}_LZ_L + \nu\bar{\nu}t_L\bar{t}_RZ_L$, $\nu\bar{\nu}t\bar{t}Z_L$ and $\nu\bar{\nu}t\bar{t}Z$. In both cases, the results in the figures confirm the estimates in Eq.(12) qualitatively, i.e. selecting helicities for $t\bar{t}$ or/and Z significantly enhances the statistical significance. Quantitatively however, there are some differences. The effects on $\nu\bar{\nu}t\bar{t}h$ are larger than naively expected, giving enhancement of close to 100% for $\nu\bar{\nu}t_R\bar{t}_Rh + \nu\bar{\nu}t_L\bar{t}_Lh$ relative to $\nu\bar{\nu}t\bar{t}h$; similarly, the enhancement for $\nu\bar{\nu}t_R\bar{t}_RZ_L + \nu\bar{\nu}t_L\bar{t}_LZ_L$ to $\nu\bar{\nu}t\bar{t}Z$ is around 300%, with the enhancement of $\nu\bar{\nu}t\bar{t}z$ largely coming from selecting Z_L . Based on the analysis above, we will specify the helicities of $t\bar{t}$ and Z to be $t_R\bar{t}_R + t_L\bar{t}_L$ and Z_L respectively in simulation and analysis for the remainder of this paper.

Finally, to have an understanding on how δy_t could be constrained if all the data from $\nu\bar{\nu}t\bar{t}h$ and $\nu\bar{\nu}t\bar{t}Z$ are sufficiently made use of. After some simple cuts and selecting helicities for the final states to be $t_R\bar{t}_R + t_L\bar{t}_L$ and Z_L , we obtain the constraints on δy_t for $\nu\bar{\nu}t\bar{t}h$, $\nu\bar{\nu}t\bar{t}Z$ and $\nu\bar{\nu}t\bar{t}h + \nu\bar{\nu}t\bar{t}Z$ respectively without decaying at 1σ and 2σ . The results are listed in Table(I). Not surprisingly, $\nu\bar{\nu}t\bar{t}h$ gives more stringent limits than $\nu\bar{\nu}t\bar{t}Z$, while the limits

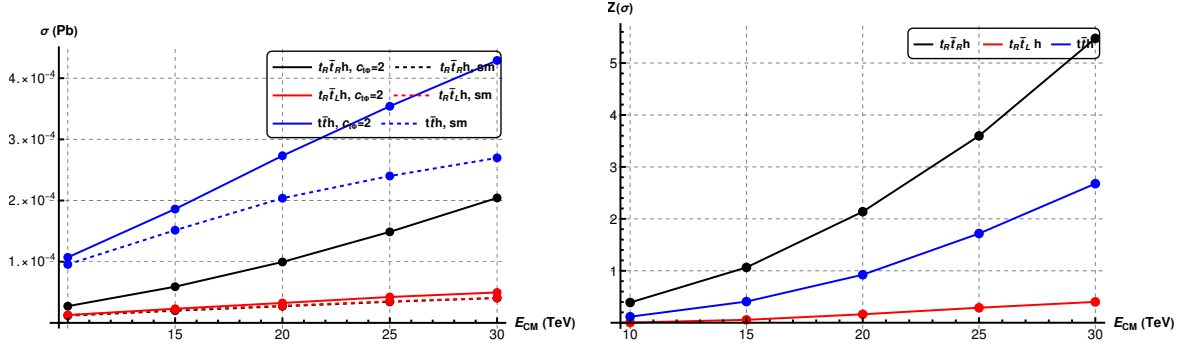


Figure 1. The figure on the left shows cross sections of $\mu\mu \rightarrow \nu\nu t\bar{t}h$ at $c_{t\phi} = 0(\text{SM})$ and $c_{t\phi} = 2(\text{BSM})$, with helicity combinations of $\nu\nu t_R\bar{t}_R h + \nu\nu t_L\bar{t}_L h$ (denoted by $t_R\bar{t}_R h$), $\nu\nu t_R\bar{t}_L h + \nu\nu t_L\bar{t}_R h$ (denoted by $t_R\bar{t}_L h$) and $\nu\nu t\bar{t}h$ (denoted by $t\bar{t}h$). No cuts are applied. The figure on the right shows the corresponding statistical significance of $t_R\bar{t}_R h$, $t_R\bar{t}_L h$ and $t\bar{t}h$.

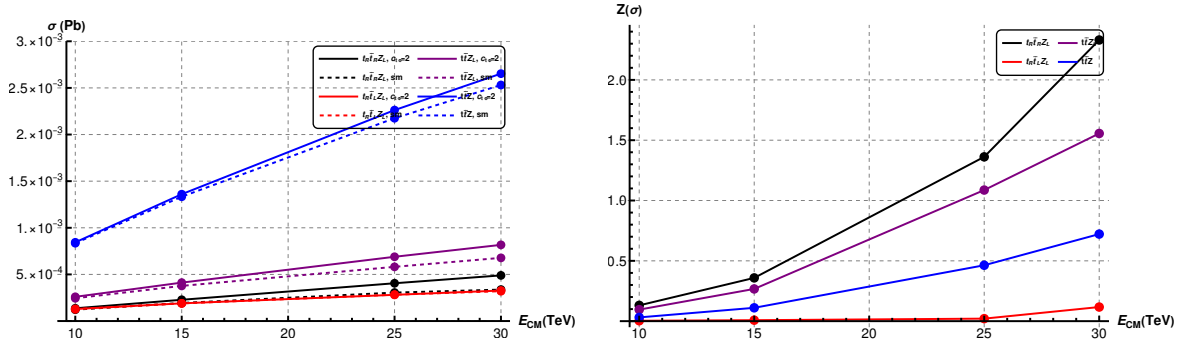


Figure 2. The figure on the left shows cross sections of $\mu\mu \rightarrow \nu\nu t\bar{t}h$ at $c_{t\phi} = 0(\text{SM})$ and $c_{t\phi} = 2(\text{BSM})$, with helicity combinations of $\nu\nu t_R\bar{t}_R Z_L + \nu\nu t_L\bar{t}_L Z_L$ (denoted by $t_R\bar{t}_R Z_L$), $\nu\nu t_R\bar{t}_L Z_L + \nu\nu t_L\bar{t}_R Z_L$ (denoted by $t_R\bar{t}_L Z_L$), $\nu\nu t\bar{t}Z_L$ (denoted by $t\bar{t}Z_L$) and $\nu\nu t\bar{t}Z$ (denoted by $t\bar{t}Z$). No cuts are applied. The figure on the right shows the statistical significance of $t_R\bar{t}_R Z_L$, $t_R\bar{t}_L Z_L$, $t\bar{t}Z_L$ and $t\bar{t}Z$.

from $\nu\nu t\bar{t}h + \nu\nu t\bar{t}Z$ are more stringent than both of them. As an example, the 1σ limit from $\nu\nu t\bar{t}h$ at 30 TeV is $[-1.0\%, 1.1\%]$, the same limit from $\nu\nu t\bar{t}Z$ is $[-0.43\%, 1.2\%]$, that from $\nu\nu t\bar{t}h + \nu\nu t\bar{t}Z$ is $[-0.36\%, 0.92\%]$. The results are comparable to ref.([21]) in which the results are obtained with bin-by-bin analysis. The results from $\nu\nu t\bar{t}Z$, which have been neglected so far in the literature, are only slightly worse than $\nu\nu t\bar{t}h$, making the combined results look particularly promising.

Channels	E_{cm}	Limits of δy_t	
		1σ	2σ
$\nu vt\bar{t}h$	30 TeV	[-1.0%, 1.1%]	[-1.1%, 1.2%]
	10 TeV	[-3.5%, 3.1%]	[-4.9%, 4.3%]
$\nu vt\bar{t}Z$	30 TeV	[-0.43%, 1.2%]	[-0.75%, 1.5%]
	10 TeV	[-2.8%, 5.2%]	[-4.4%, 6.7%]
$\nu vt\bar{t}h + \nu vt\bar{t}Z$	30 TeV	[-0.36%, 0.92%]	[-0.73%, 1.2%]
	10 TeV	[-2.6%, 3.1%]	[-3.7%, 4.3%]

Table I: The constraints on δy_t for $\nu vt\bar{t}h$, $\nu vt\bar{t}Z$ and $\nu vt\bar{t}h + \nu vt\bar{t}Z$ respectively without decaying. The helicities of $t\bar{t}$ are selected to be $t_R\bar{t}_R + t_L\bar{t}_L$, the helicity of Z to be Z_L . To $\nu vt\bar{t}h$ we applied the cuts of $p_T(t) > 200$ GeV and $p_T(h) > 100$ GeV; to $\nu vt\bar{t}Z$ we applied the cuts of $p_T(t) > 200$ GeV, $p_T(Z) > 250$ GeV.

III. FULL ANALYSIS OF $\nu vt\bar{t}h$

In this section, we carry out a detailed analysis on the lepton channel $l^+l^-2b + \text{MET}$ and the semi-lepton channel $l^\pm jj4b + \text{MET}$, both of which come mainly from $\nu vt\bar{t}h$, with minor contribution from $\nu vt\bar{t}Z$. Same as in parton processes, we simulate with hard processes with Madgraph5_3_4_1 and SMEFTatNLO_LO. We also decay heavy particles with Madspin. However, since muon colliders are not built yet, we deem it premature to do collider analysis, thus we don't implement parton shower and hadronization in our simulation. Nonetheless we believe simulation and analysis on the parton level is enough to obtain relatively reliable results. To take into account of those effects, we set b tagging efficiency to be 0.9. We will also scan the tagging efficiencies of Z_L and $t_R\bar{t}_R/t_L\bar{t}_L$ in the analysis to see how our results varies with taggin efficiencies. For the other settings we follow Sec.(II B), the formula of statistical significance is given by Eq.(13). For c.m. energy and integrated luminosity, we use Eq.(16) choose 10 ab^{-1} at 10 TeV and 90 ab^{-1} at 30 TeV as two benchmark points.

A. Lepton Channel

In this subsection we will study the channel $l^+l^-4b + \text{MET}$ with $l = e, \mu$ and $b = b/\bar{b}$ of which the dominant contribution comes from $\nu vt\bar{t}h$ process, but minor contribution also

come from $\nu\nu ttZ$. It's obtained from the hard process through $t \rightarrow bW^+ \rightarrow bl^+\nu_l$, $\bar{t} \rightarrow \bar{b}W^- \rightarrow \bar{b}l^-\bar{\nu}_l$, $h/Z \rightarrow b\bar{b}$. When analyzing data, we will always include contributions from $\nu\nu tth$, but also include $\nu\nu ttZ$ when it's beneficial to do so.

The main background processes are

$$\begin{aligned}
\mu\mu &\rightarrow \nu\bar{\nu}t_R\bar{t}_Rh/Z_L(\text{SM}) \rightarrow 2\nu 2\bar{\nu}l^+l^-4b \\
\mu\mu &\rightarrow t_R\bar{t}_Rh \rightarrow \nu\bar{\nu}l^+l^-4b \\
\mu\mu &\rightarrow \nu\bar{\nu}Z_LZ_LZ_L \rightarrow \nu\bar{\nu}l^+l^-4b \\
\mu\mu &\rightarrow \nu\bar{\nu}Z_LZ_Lh \rightarrow \nu\bar{\nu}l^+l^-4b \\
\mu\mu &\rightarrow \nu\bar{\nu}Z_Lhh \rightarrow \nu\bar{\nu}l^+l^-4b \\
\mu\mu &\rightarrow l^+\nu_lW^-Z_LZ_L(/l^-\bar{\nu}_lW^+Z_LZ_L) \rightarrow \nu\bar{\nu}l^+l^-4b \\
\mu\mu &\rightarrow l^+\nu_lW^-Z_Lh(/l^-\bar{\nu}_lW^+Z_Lh) \rightarrow \nu\bar{\nu}l^+l^-4b \\
\mu\mu &\rightarrow l^+\nu_lW^-hh(/l^-\bar{\nu}_lW^+hh) \rightarrow \nu\bar{\nu}l^+l^-4b
\end{aligned} \tag{17}$$

with $t_R\bar{t}_R$ denoting $t_R\bar{t}_R + t_L\bar{t}_L$. There are also other background processes, such as $t\bar{t}Z$, ZZZ and etc, but their cross sections are all negligible compared with those listed above. The largest contribution to background is $\nu\bar{\nu}tth/Z$ from SM.

1. 30 TeV

We first study 30 TeV for the lepton channel from $\nu\nu tth$. For all the processes, we implement a set of preliminary cuts:

$$p_T(b) > 20 \text{ GeV}, \quad p_T(l) > 30 \text{ GeV} \tag{18}$$

with $b = b/\bar{b}$ and $l = l^+/l^-$. We emphasize again that the crucial setting of our analysis is specifying helicities of final particles. To accommodate collider environment, we will scan over different values of spin tagging efficiencies of Z and t/\bar{t} from 1 to 0.6, in doing analysis.

To reduce background and increase statistical significance, we apply some cuts on the events, which are summarized as following:

- Cut 1: Reject $70 \text{ GeV} < M_{l+l^-} < 115 \text{ GeV}$. The purpose of this cut is to reduce event numbers of processes such as $\nu\bar{\nu}Z_LZ_LZ_L$ that have Z decaying into l^+l^- .

- Cut 2: Reject $\eta(l^+) > 3$; select $M_{bl^+} < 250$ GeV, select $M_{bl^-} < 250$ GeV. The purpose of this cut is to reduce event numbers of processes such as $l^+\nu_l W^+ Z_L Z_L$ that have leptons with large rapidity and have no top quark as an intermediate state.
- Cut 3: Select $p_T(b) > 50$ GeV, select $p_T(l) > 50$ GeV, select MET > 30 GeV. The purpose of this cut is to reduce the SM part of signal processes $\nu\bar{\nu}t_R\bar{t}_R h/Z_L$ and $\nu\bar{\nu}t_L\bar{t}_L h/Z_L$.

with $b = b/\bar{b}$ and $l = l^+/l^-$. The results of the cut flow are summarized in Table(II). In Fig.(3), we also show some plots such as $p_T(l^+)$ before and after cuts to demonstrate the effects of our method.

After obtaining the final results after cuts, combined with b tagging efficiency $\epsilon_b = 0.9$ and spin tagging efficiencies ϵ_s , we can obtain the corresponding statistical significance Z . Taking $\epsilon_s = 0.9$ (for all particles with helicities selected) as an example, following Eq.(13), we obtain $Z = 22.8(\sigma)$ if combining events of $\nu\bar{\nu}tth$ and $\nu\bar{\nu}ttz$. This is an encouraging result. Following the same procedure we can obtain the constraint on $c_{t\phi}(\Lambda = 1$ TeV) with $\epsilon_s = 0.9$ as $-0.56 \leq c_{t\phi} \leq 0.53$ at 2σ and $-0.43 \leq c_{t\phi} \leq 0.5$ at 1σ . Converting them into constraints on δy_t (Eq.(8)), we get $-3.2\% \leq \delta y_t \leq 3.4\%$ at 2σ and $-3.1\% \leq \delta y_t \leq 2.6\%$ at 1σ . The results are quite promising.

Finally, the technique for tagging the spins of a particle is not yet mature and subject to variation for different processes, thus we analyze how statistical significance Z changes with spin tagging efficiency ϵ_s , as well as with $c_{t\phi}$. For the values of ϵ_s , we set equal for that of Z and t/\bar{t} and scan over 1, 0.9, 0.8, 0.7, 0.6. The results are summarized in Fig(4). The results show that the statistical significance remains high when spin tagging efficiency varies, even when reaching as low as $\epsilon_s = 0.6$. We also compute the limits of δy_t at $\epsilon_s = 0.7$, the results are summarized with $\epsilon_s = 0.9$ and other processes in Table(VIII).

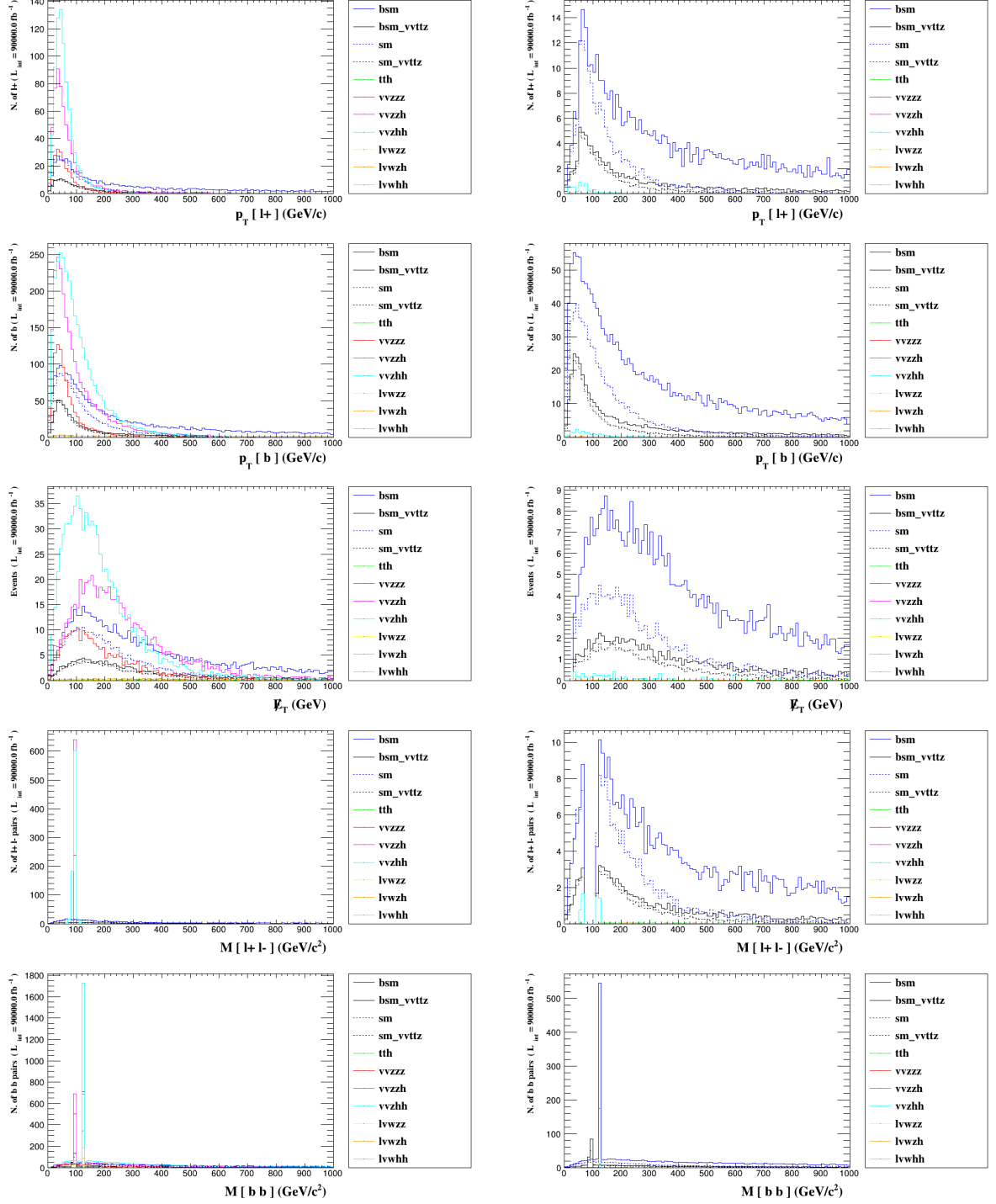


Figure 3. Distributions of the lepton channel of νtth at 30 TeV before(left) and after(right) cuts (see Item(III A 1)), see also Table(II) for event numbers with the cut flow.

process	before cuts	cut1	cut2	cut3
BSM($\nu\bar{\nu}t_R\bar{t}_R h/\nu\bar{\nu}t_L\bar{t}_L h$)	675.9×2	610.8×2	554.3×2	524.3×2
BSM($\nu\bar{\nu}t_R\bar{t}_R Z_L/\nu\bar{\nu}t_L\bar{t}_L Z_L$)	167.3×2	143.8×2	119.2×2	107.9×2
SM($\nu\bar{\nu}t_R\bar{t}_R h/\nu\bar{\nu}t_L\bar{t}_L h$)	312.6×2	248.8×2	189.9×2	159.1×2
SM($\nu\bar{\nu}t_R\bar{t}_R Z_L/\nu\bar{\nu}t_L\bar{t}_L Z_L$)	117.4×2	94.8×2	71.3×2	60.3×2
$t_R\bar{t}_R h/t_L\bar{t}_L h$	10.5×2	10.5×2	10.5×2	10.5×2
$\nu\bar{\nu}Z_L Z_L Z_L$	237.8	0	0	0
$\nu\bar{\nu}Z_L Z_L h$	639.6	0	0	0
$\nu\bar{\nu}Z_L h h$	832.5	12.15	6.9	5.3
$l^\pm\nu W^\mp Z_L Z_L$	8.0×2	7.8×2	0.7×2	0.7×2
$l^\pm\nu W^\mp Z_L h$	89.3×2	88.6×2	1.3×2	1.3×2
$l^\pm\nu W^\mp h h$	91.874×2	91.3×2	0.7×2	0.7×2

Table II: Cut flow of the lepton channel of $\nu\nu tth$ at 30 TeV with integrated luminosity 90 ab^{-1} . BSM processes are set at $c_{t\phi} = 2$ (with $\Lambda = 1\text{ TeV}$). Helicity selections are shown in the table. The b tagging efficiency and spin tagging efficiencies ϵ_s are set to be is

$$\epsilon_b = \epsilon_s = 1.$$

2. 10 TeV

We now turn to 10 TeV for the lepton channel from $\nu\nu tth$. We impose the following cuts to reduce background:

- Cut 1: Reject $70\text{ GeV} < M_{l+l^-} < 115\text{ GeV}$, reject $\text{MET} > 650\text{ GeV}$
- Cut 2: Select $p_T(b) > 50\text{ GeV}$, select $p_T(l) > 50\text{ GeV}$.

with $b = b/\bar{b}$ and $l = l^+/l^-$.

The cuts on 10 TeV is modified slightly relative to 30 TeV of the same channel: Cut 1 is to reduce background processes, while Cut 2 is to optimize signals relative to their SM counter parts. The cut flow of the signal and background processes at $c_{t\phi} = 2(\Lambda = 1\text{ TeV})$ is summarized in Table(III). Using the cuts in Item(III A 2) and setting the spin tagging efficiency to be 0.9, δ_{y_t} is constrained to be within $[-11.0\%, 9.8\%]$ at 1σ level. At 2σ level, didn't take the precise value, since we have $|c_{t\phi}| > 2$ ($|\delta_{y_t}| > 12.2\%$).

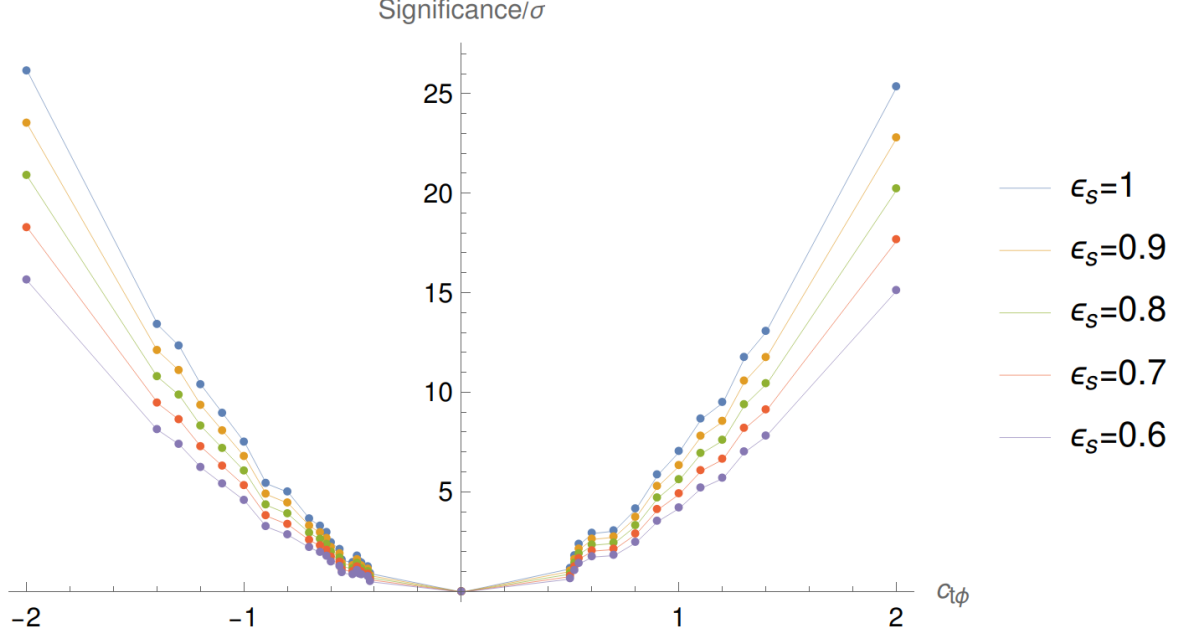


Figure 4. The dependence of statistical significance of the lepton channel of $\nu\bar{\nu}t\bar{t}h$ at 30 TeV (Item(III A 1)) on $c_{t\phi}$ ($\Lambda = 1$ TeV) and spin tagging efficiency ϵ_s . Z boson and t/\bar{t} take the same value on ϵ_s . The b quark tagging efficiency is set to be $\epsilon_b = 0.9$.

B. Semi-Lepton Channel

In this subsection, we study the channel $l^\pm jj4b + \text{MET}$ with $l = e, \mu$, which has contributions from both $\nu\bar{\nu}t\bar{t}h$ and $\nu\bar{\nu}t\bar{t}Z$, but $\nu\bar{\nu}t\bar{t}h$ is the dominant process. It's obtained through $t \rightarrow bW^+ \rightarrow bl^+\nu_l$, $\bar{t} \rightarrow \bar{b}W^- \rightarrow \bar{b}j\bar{j}$, $h/Z_L \rightarrow b\bar{b}$; or $t \leftrightarrow \bar{t}$. As usual, we choose the helicities of t, \bar{t} and Z boson to be $t_R\bar{t}_R/t_L\bar{t}_L$ and Z_L respectively, while the helicities of W^\pm are not tagged. The spin tagging efficiencies of all particles are set to be the same.

The main background processes are

$$\mu\mu \rightarrow \nu\bar{\nu}t_R\bar{t}_R h/Z_L(\text{SM}) \rightarrow 3\nu l^\pm 4bjj \quad (19)$$

$$\mu\mu \rightarrow t_R\bar{t}_R h/Z_L \rightarrow 2\nu l^\pm 4bjj \quad (20)$$

$$\mu\mu \rightarrow l^+\nu_l W^- Z_L Z_L (/l^-\bar{\nu}_l W^+ Z_L Z_L) \rightarrow \nu l^\pm 4bjj \quad (21)$$

$$\mu\mu \rightarrow l^+\nu_l W^- Z_L h (/l^-\bar{\nu}_l W^+ Z_L h) \rightarrow \nu l^\pm 4bjj \quad (22)$$

$$\mu\mu \rightarrow l^+\nu_l W^- hh (/l^-\bar{\nu}_l W^+ hh) \rightarrow \nu l^\pm 4bjj \quad (23)$$

1. 30 TeV

We start with c.m. energy of 30 TeV. The semi-lepton channel has a much larger cross-section than lepton channel due to the larger branching ratio of $W \rightarrow jj$. With the increase of luminosity and smaller number of background processes, we expect a high significance and stringent limit on δy_t .

As summarized as below, we apply the following cuts to reduce background and increase statistical significance:

- Cut 1: reject $p_T(l) < 20$ GeV. This cut reduces both SM and BSM events of $\nu tth/Z$ equally, therefore enhancing the signal relative to the background.
- Cut 2: select $p_T(b) < 700$ GeV, reject $1.7 < \eta(l^+) < 2.5$. This cut reduces $lvwzh$ and $lvwhh$, as well as the SM part of νtth and νttz .

process	before cuts	cut1	cut2
BSM($\nu\bar{\nu}t_R\bar{t}_Rh/\nu\bar{\nu}t_L\bar{t}_Lh$)	15.3×2	9×2	8.1×2
BSM($\nu\bar{\nu}t_R\bar{t}_RZ_L/\nu\bar{\nu}t_L\bar{t}_LZ_L$)	5.1×2	2.6×2	2.2×2
SM($\nu\bar{\nu}t_R\bar{t}_Rh/\nu\bar{\nu}t_L\bar{t}_L$)	11.2×2	5.6×2	4.7×2
SM($\nu\bar{\nu}t_R\bar{t}_RZ_L/\nu\bar{\nu}t_L\bar{t}_LZ_L$)	4.6×2	2.2×2	1.8×2
$t_R\bar{t}_Rh/t_L\bar{t}_Lh$	7.4×2	2.6×2	2.6×2
$t_R\bar{t}_RZ_L/t_L\bar{t}_LZ_L$	1.3×2	0.6×2	0.5×2
$\nu\bar{\nu}Z_LZ_LZ_L$	8.6	0	0
$\nu\bar{\nu}Z_LZ_Lh$	22.9	0	0
$\nu\bar{\nu}Z_Lhh$	31.2	0.3	0.2
$lvwzz$	1.7	0.3	0.3
$lvwzh$	5.0	1.3	1.3
$lvwhh$	6.1	2.0	2.0

Table III: Cut flow of lepton channel of νtth at 10 TeV with integrated luminosity $10 ab^{-1}$. BSM processes are simulated at $c_{t\phi} = 2$ (with $\Lambda = 1$ TeV). Helicity selections are shown in the table. Processes with negligible cross sections are not listed. The b tagging efficiency and spin tagging efficiencies ϵ_s are set to be $\epsilon_b = \epsilon_s = 1$.

process	before cuts	cut1	cut2	cut3
BSM($\nu\bar{\nu}t_R\bar{t}_Rh/\nu\bar{\nu}t_L\bar{t}_Lh$)	2025×4	1963.41×4	1695.2×4	1239.2 ×4
BSM($\nu\bar{\nu}t_R\bar{t}_RZ_L/\nu\bar{\nu}t_L\bar{t}_LZ_L$)	505×4	481.30×4	405.14 ×4	257.0 ×4
SM($\nu\bar{\nu}t_R\bar{t}_Rh/\nu\bar{\nu}t_L\bar{t}_Lh$)	884×4	829.1×4	706.5 ×4	333.5 ×4
SM($\nu\bar{\nu}t_R\bar{t}_RZ_L/\nu\bar{\nu}t_L\bar{t}_LZ_L$)	352×4	329.55×4	273.86 ×4	135.32 ×4
$t_R\bar{t}_Rh/t_L\bar{t}_Lh$	32.2×4	32.181×4	17.49 ×4	16.36 ×4
$t_R\bar{t}_RZ_L/t_L\bar{t}_LZ_L$	5.66×4	5.6557 ×4	2.64 ×4	2.48 ×4
$l^\pm\nu W^\mp Z_L Z_L$	22.3×2	22.259 ×2	4.39 ×2	3.13 ×2
$l^\pm\nu W^\mp Z_L h$	273×2	272.42 ×2	61.77 ×2	55.85 ×2
$l^\pm\nu W^\mp hh$	304×2	304.15 ×2	171.99 ×2	168.9 ×2

Table IV: Cut flow of the semi-lepton channel of $\nu\bar{\nu}tth$ at 30 TeV, with integrated luminosity 90 ab^{-1} . BSM processes are simulated at $c_{t\phi} = 2$ (with $\Lambda = 1\text{ TeV}$). Helicity selections are shown in the table. The b tagging efficiency and spin tagging efficiencies ϵ_s are set to be is $\epsilon_b = \epsilon_s = 1$.

- Cut 3: select $-2 < \eta(b) < 2$, reject $M(bjj) < 200\text{ GeV}$, reject $\text{MET} < 20\text{ GeV}$. In this cut we continue to optimize the results by reducing SM of $\nu\bar{\nu}tth/z$.

with $b = b/\bar{b}$ and $l = l^+/l^-$. The results of the cut flow are summarized in Table(IV), with which we can then obtain the corresponding statistical significance Z . Taking $\epsilon_s = 0.9$ (and $\epsilon_b = 0.9$), following Eq.(13), we obtain $Z = 50.27(\sigma)$ at $c_{t\phi} = 2$ and $\Lambda = 1\text{ TeV}$ if combining $\nu\bar{\nu}tth$ and $\nu\bar{\nu}ttz$. We also show some plots of the events before and after the cuts in Fig.(5). Following the same procedure we can obtain the constraint on $C_{t\phi} \equiv \frac{c_{t\phi}}{\Lambda^2}$ with $\epsilon_s = 0.9$ as $-0.61\text{ TeV}^{-2} \leq C_{t\phi} \leq 0.625\text{ TeV}^{-2}$ at 5σ , $-0.45\text{ TeV}^{-2} \leq C_{t\phi} \leq 0.405\text{ TeV}^{-2}$ at 2σ and $-0.3\text{ TeV}^{-2} \leq C_{t\phi} \leq 0.27\text{ TeV}^{-2}$ at 1σ . Converting them into constraints on δy_t using Eq.(8), we get $-3.8\% \leq \delta y_t \leq 3.7\%$ at 5σ , $-2.5\% \leq \delta y_t \leq 2.7\%$ at 2σ and $-1.6\% \leq \delta y_t \leq 1.8\%$ at 1σ . As we can see, the results are visibly better than the lepton channel.

Finally, we analyze how statistical significance Z changes with spin tagging efficiency ϵ_s , as well as with $c_{t\phi}$. The results are summarized in Fig(6).

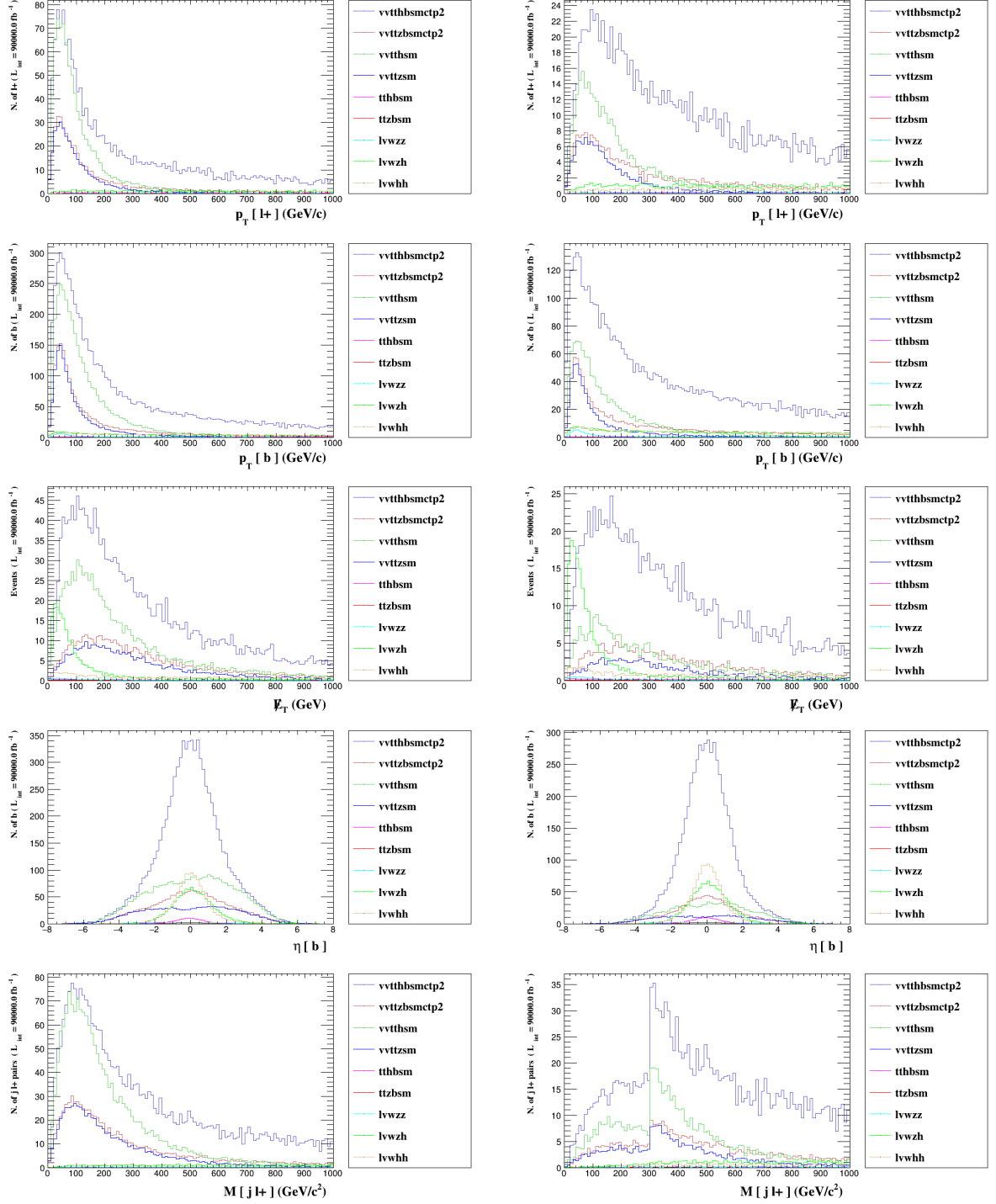


Figure 5. Distributions of the semi-lepton channel $\nu t t h$ at 30 TeV before(left) and after(right) cuts (Item(III B1)), see also Table(IV) for event numbers with the cut flow.

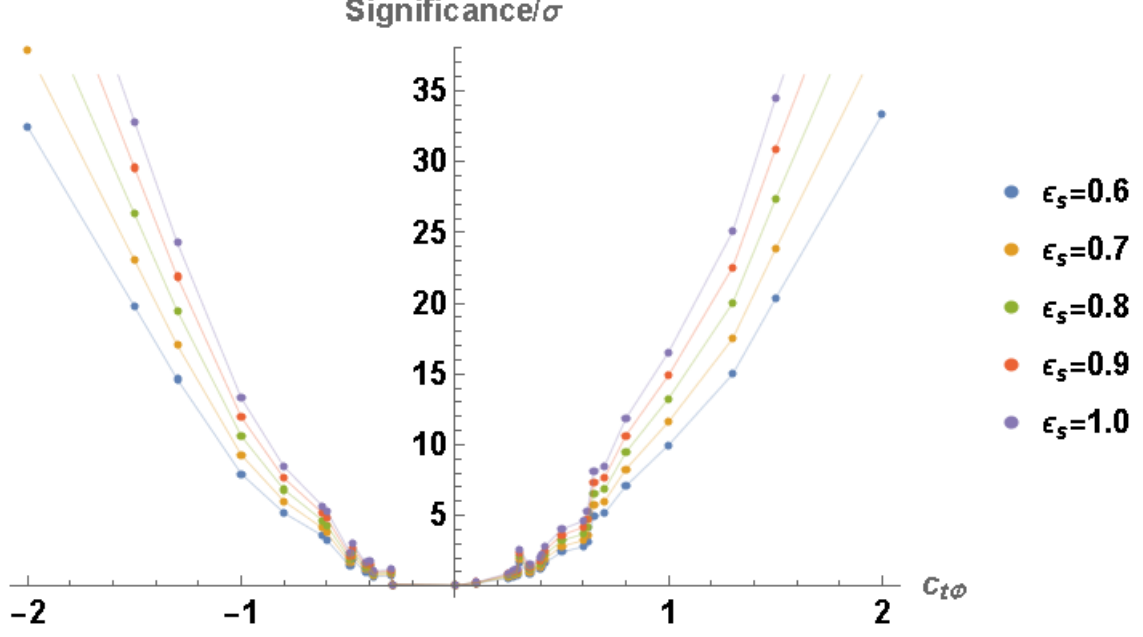


Figure 6. The dependence of statistical significance of the semi-lepton channel $\nu vtth$ at 30 TeV on $c_{t\phi}$ (with $\Lambda = 1$ TeV) and spin tagging efficiency ϵ_s , the latter of Z and t/\bar{t} are take to be the equal. The b quark tagging efficiency is set to be $\epsilon_b = 0.9$.

2. 10 TeV

We then proceed to 10 TeV for the semi-lepton channel of $\nu vtth$. The cuts we applied to reduce background and increase statistical significance are summarized as follows:

- Cut 1: Select $-2 < \eta(b) < 2$, Select $M_{l+l^-} > 300$ GeV, Select $M_{bj} > 200$ GeV. The purpose of this cut is to reduce the SM part of signal processes $\nu\bar{\nu}t_R\bar{t}_Rh/Z_L$ and $\nu\bar{\nu}t_L\bar{t}_Lh/Z_L$.
- Cut 2: Select $2 < \Delta R_{l+,j} < 4$, $\Delta R_{l+,b} > 4$, $1 < \Delta R_{b,j} < 4$. The purpose of this cut is to reduce the contribution from processes such as $l^+\nu_l W^+ Z_L Z_L$, $l^+\nu_l W^+ Z_L h$, $l^+\nu_l W^+ hh$ which typically produce leptons with large rapidity and do not involve top quarks as intermediate states. This selection helps isolating the signal processes of interest by removing events where the lepton-jet separation $\Delta R_{l+,j}$ is either too small or too large, and ensuring that the lepton-b quark separation $\Delta R_{l+,b}$ is sufficiently large to exclude non-top quark background. Additionally, requiring $1 < \Delta R_{b,j} < 4$ helps suppressing background from SM processes and $t\bar{t}h$ production.

process	before cuts	cut1	cut2	cut3
BSM($\nu\bar{\nu}t_R\bar{t}_Rh/\nu\bar{\nu}t_L\bar{t}_Lh$)	45.3×4	19.67×4	14.61×4	12.2×4
BSM($\nu\bar{\nu}t_R\bar{t}_RZ_L/\nu\bar{\nu}t_L\bar{t}_LZ_L$)	15.4×4	5.41×4	2.79×4	2.18×4
SM($\nu\bar{\nu}t_R\bar{t}_Rh/\nu\bar{\nu}t_L\bar{t}_Lh$)	33.7×4	9.02×4	5.29 ×4	4.15×4
SM($\nu\bar{\nu}t_R\bar{t}_RZ_L/\nu\bar{\nu}t_L\bar{t}_LZ_L$)	13.7×4	3.91×4	1.61 ×4	1.23×4
$t_R\bar{t}_Rh/t_L\bar{t}_Rh$	22.1×4	20.5×4	13.59 ×4	6.07×4
$t_R\bar{t}_RZ_L/t_L\bar{t}_LZ_L$	3.93×4	3.727 ×4	2.612 ×4	1.14×4
$l\nu W Z_L Z_L$	4.62×2	3.499 ×2	0.79 ×2	0.354×2
$l\nu W Z_L h$	14.7×2	11.77 ×2	4.14 ×2	1.97×2
$l\nu W h h$	19.5×2	15.85 ×2	7.48 ×2	3.96×2

Table V: Cut flow of the semi-lepton channel of $\nu t \bar{t} h$ at 10 TeV, with integrated luminosity 10 ab^{-1} . BSM processes are simulated at $c_{t\phi} = 2$ (with $\Lambda = 1 \text{ TeV}$). Helicity selections are shown in the table. The b tagging efficiency and spin tagging efficiency are set to be $\epsilon_b = \epsilon_s = 1$.

- Cut 3: Select $p_T(l^+) > 60 \text{ GeV}$, Select $800 \text{ GeV} < p_T(j) < 1000 \text{ GeV}$, Select $\eta(l) > 2$. Without rejecting a large number of signal events, it make some cuts and optimize the significance.

with $b = b/\bar{b}$ and $l = l^+/l^-$. The results of the cut flow are summarized in Table(V), according to which we can obtain the corresponding statistical significance Z . The b tagging efficiency and spin tagging efficiency are set to be $\epsilon_b = \epsilon_s = 0.9$ (for all particles with helicities specified) and following Eq.(13), we obtain $Z = 3.2(\sigma)$ at $C_{t\phi} = 2 \text{ TeV}^{-1}$. Following the same procedure as the previous sections, we can obtain the constraint on $c_{t\phi}$ with $\epsilon_s = 0.9$ as $-1.6 \leq c_{t\phi} \leq 1.6$ at 2σ and $-1.1 \leq c_{t\phi} \leq 1.15$ at 1σ with $\Lambda = 1 \text{ TeV}$. Converting them into constraints on δy_t , we get $-9.8\% \leq \delta y_t \leq 9.8\%$ at 2σ and $-7.0\% \leq \delta y_t \leq 6.7\%$ at 1σ . We also show some plots of the events before and after the cuts in Fig.(7).

Finally, we analyze how statistical significance Z changes with spin tagging efficiency ϵ_s and $c_{t\phi}$. For the values of ϵ_s , we set equal for that of Z and t/\bar{t} and scan over 1, 0.9, 0.8, 0.7, 0.6. The results are summarized in Fig(8).

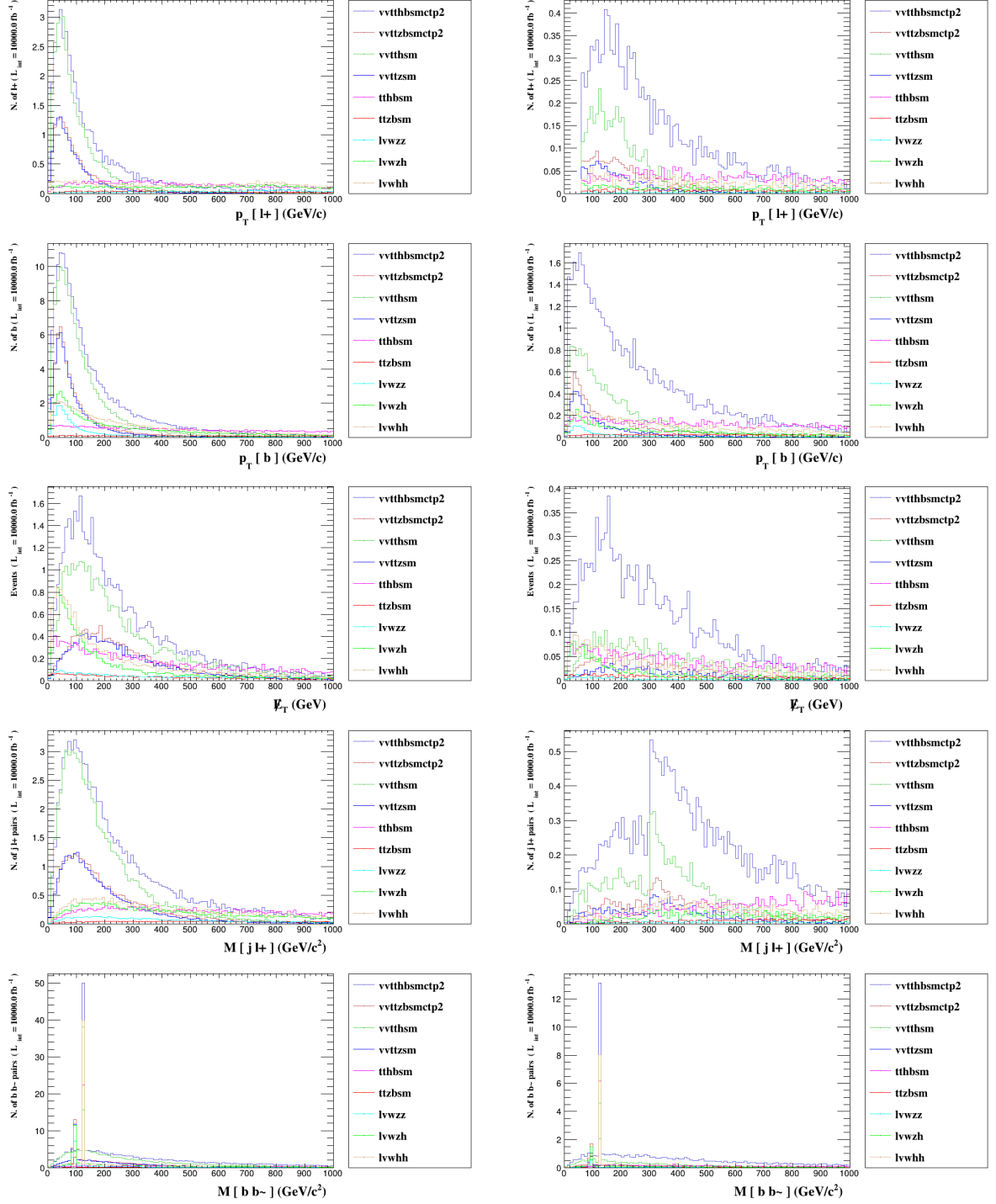


Figure 7. Distributions of the semi-lepton channel from $\nu t th$ at 10 TeV before(left) and after(right) cuts (Item(III B 2)), see also Table(V) for event numbers with the cut flow. The b tagging efficiency and spin tagging efficiency are set to be $\epsilon_b = \epsilon_s = 1$.

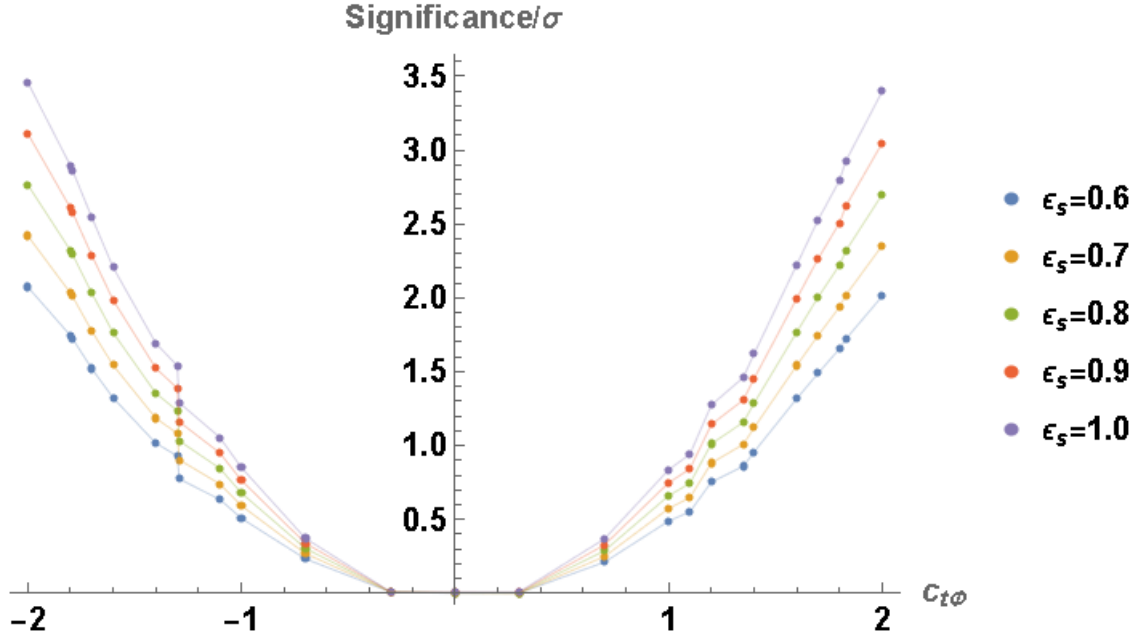


Figure 8. The dependence of statistical significance of the semi-lepton channel of $\nu\nu tth$ at 10 TeV on $c_{t\phi}$ (with $\Lambda = 1$ TeV) and spin tagging efficiency ϵ_s , the latter of Z and t/\bar{t} are take to be equal. The b quark tagging efficiency is set to be $\epsilon_b = 0.9$.

IV. FULL ANALYSIS OF $\nu\nu tZ$

In this section we analyze the lepton channel of $2(l^+l^-)2b + \text{MET}$ and the semi-lepton channel of $3l^\pm jj2b + \text{MET}$ with $l = e, \mu$, $b = b/\bar{b}$, which come from $\nu\nu tZ$ and $\nu\nu tth$, but dominated by the former. Our simulation strategy and settings are the same as Sec.(II B and III), so we won't repeat here.

A. Lepton Channel

In this subsection, we study the channel $2(l^+l^-)2b + \text{MET}$, which comes from $\nu\nu tZ$ only through $t \rightarrow bW^+ \xrightarrow{W^+ \rightarrow l^+\nu_l} bl^+\nu_l$, $\bar{t} \rightarrow \bar{b}W^- \xrightarrow{W^- \rightarrow l^-\bar{\nu}_l} \bar{b}l^-\bar{\nu}_l$ and $Z \rightarrow l^+l^-$. $\nu\nu tth$ has a negligible contribution in this channel, since the probability of $h \rightarrow l^+l^-$ is close to 0.

The main background processes are

$$\begin{aligned}
\mu\mu &\rightarrow \nu\bar{\nu}t_L\bar{t}_L/\nu\bar{\nu}t_R\bar{t}_R Z_L(\text{SM}) \rightarrow 2\nu 2\bar{\nu}2(l^+l^-)2b \\
\mu\mu &\rightarrow t_L\bar{t}_L/t_R\bar{t}_R Z_L \rightarrow \nu\bar{\nu}2(l^+l^-)2b \\
\mu\mu &\rightarrow \nu\bar{\nu}Z_L Z_L Z_L \rightarrow \nu\bar{\nu}2(l^+l^-)2b \\
\mu\mu &\rightarrow \nu\bar{\nu}Z_L Z_L h \rightarrow \nu\bar{\nu}2(l^+l^-)2b \\
\mu\mu &\rightarrow l^+\nu_l W^- Z_L Z_L(/l^-\bar{\nu}_l W^+ Z_L Z_L) \rightarrow \nu\bar{\nu}2(l^+l^-)2b \\
\mu\mu &\rightarrow l^+\nu_l W^- Z_L h(/l^-\bar{\nu}_l W^+ Z_L h) \rightarrow \nu\bar{\nu}2(l^+l^-)2b
\end{aligned} \tag{24}$$

of which the largest contribution to the background is $\nu\bar{\nu}ttZ$ from SM. Processes with negligible cross sections are not listed. We only give the results of 30 TeV, since the limits on δy_t at 10 TeV is too weak ($|C_{t\phi}| < 2 \text{ TeV}^{-1}$).

30 TeV

For all the processes, we implement a set of preliminary cuts:

$$p_T(l) > 40 \text{ GeV}, \quad p_T(b) > 40 \text{ GeV} \tag{25}$$

with $b = b/\bar{b}$ and $l = l^+/l^-$.

The cuts we apply on the events are summarized as following:

- Cut 1: Reject $80 \text{ GeV} < M_{b_1 b_2} < 100 \text{ GeV}$; Reject $120 \text{ GeV} < M_{b_1 b_2} < 130 \text{ GeV}$. The purpose of these cuts is to reduce the processes such as $\nu\bar{\nu}ZZZ$, $\nu\bar{\nu}ZZh$, $l^+\nu_l W^+ Zh$ that have Z and h decaying to $2b$.
- Cut 2: Reject $p_T(l) > 40 \text{ GeV}$; Reject $p_T(b) > 40 \text{ GeV}$. The purpose of these cuts is to reduce the SM part of signal process $\nu\bar{\nu}t\bar{t}Z$.
- Cut 3: Reject $\eta(l^+) < -3$ and $\eta(l^+) > 3$; Reject $\eta(b) < -3$ and $\eta(b) > 3$. The purpose of these cuts is also to reduce the SM part of signal process.

The results of the cut flow are summarized in Table(VI), according to which, combined with b tagging efficiency $\epsilon_b = 0.9$ and spin tagging efficiency ϵ_s , we can obtain the corresponding statistical significance Z . Taking $\epsilon_s = 0.9$ and following Eq.(13), we obtain $Z = 6.0(\sigma)$ at $c_{t\phi} = 2$ with $\Lambda = 1 \text{ TeV}$. We also show some plots of the events before and

process	before cuts	cut1	cut2	cut3
BSM($\nu\bar{\nu}t_R\bar{t}_R Z_L/\nu\bar{\nu}t_L\bar{t}_L Z_L$)	76.567×2	71.54×2	25.08×2	21.22×2
SM($\nu\bar{\nu}t_R\bar{t}_R Z_L/\nu\bar{\nu}t_L\bar{t}_L Z_L$)	53.402×2	48.74×2	7.26×2	3.97×2
$t_R\bar{t}_R Z_L/t_L\bar{t}_L Z_L$	0.8574×2	0.8532×2	0.794×2	0.785×2
$\nu\bar{\nu}h Z_L Z_L$	105.676	0	0	0
$\nu\bar{\nu} Z_L Z_L Z_L$	53.399	2.61	0.402	0.172
$l\nu_l W Z_L Z_L$	6.7635×2	0.362×2	0.177×2	0.151×2
$l\nu_l W h Z_L$	41.633×2	0	0	0

Table VI: Cut flow of the lepton channel of $\nu\bar{\nu}t\bar{t}z$ at 30 TeV, integrated luminosity is 90 ab^{-1} . The BSM process is simulated at $c_{t\phi} = 2$ (with $\Lambda = 1\text{ TeV}$). Helicity selections are shown in the table. Background processes that have negligible contribution are not listed.

The b tagging efficiency and spin tagging efficiency are set to be $\epsilon_b = \epsilon_s = 1$.

after the cuts in Fig.(9). We also obtain the constraint on $c_{t\phi}$ with $\Lambda = 1\text{ TeV}$ at $\epsilon_s = 0.9$ as $-1.2 \leq c_{t\phi} \leq 1.1$ at 2σ and $-0.95 \leq c_{t\phi} \leq 0.9$ at 1σ . Converting them into constraints on δy_t , we get $-6.7\% \leq \delta y_t \leq 7.3\%$ at 2σ and $-5.5\% \leq \delta y_t \leq 5.8\%$ at 1σ .

We analyze how statistical significance Z changes with spin tagging efficiency ϵ_s , as well as with $c_{t\phi}$. For the values of ϵ_s , we set them equal for Z and t/\bar{t} , then scan over 1, 0.9, 0.8, 0.7, 0.6. The results are summarized in Fig.(10).

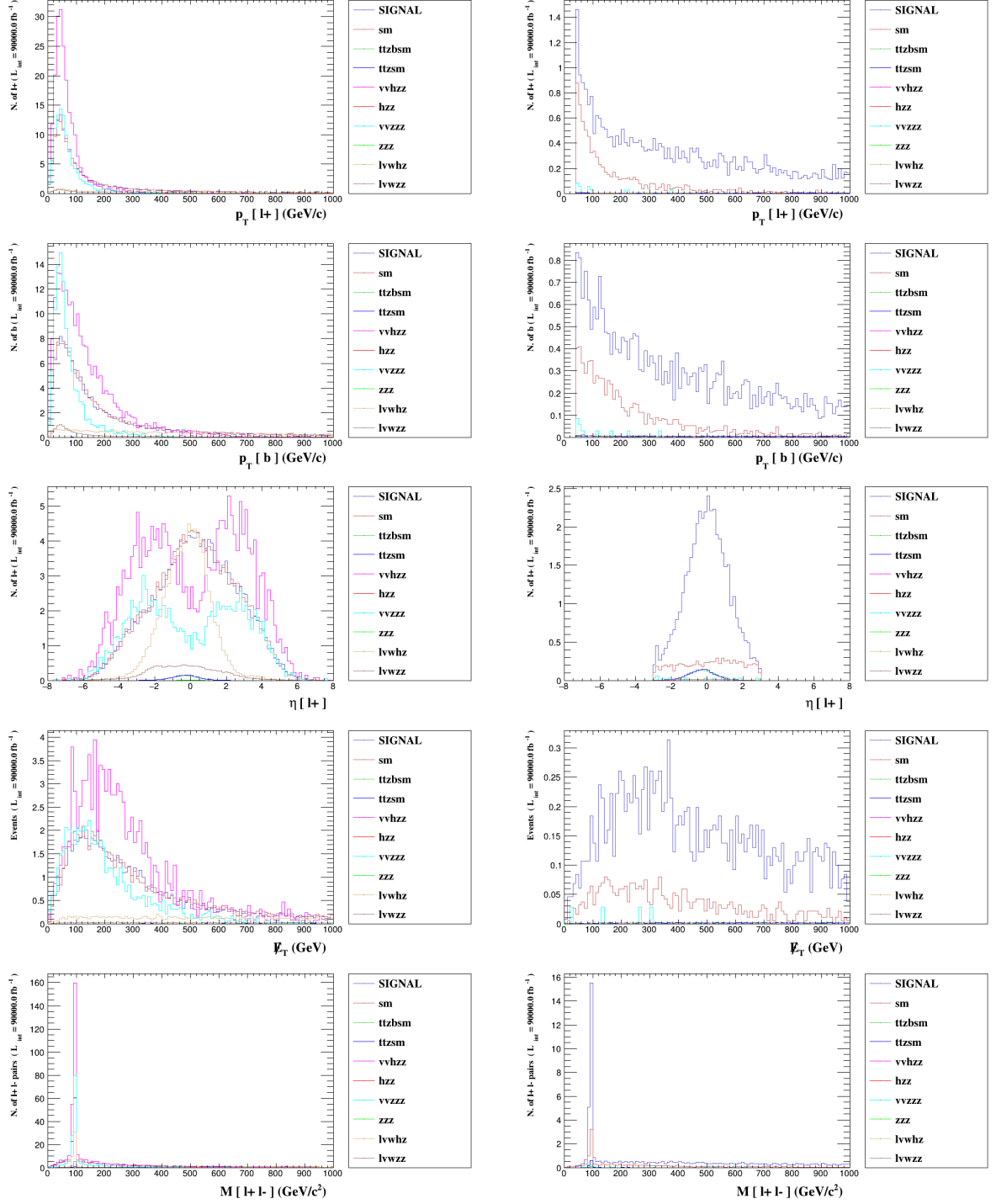


Figure 9. Distributions of the lepton channel of $\nu\bar{\nu}t\bar{t}Z$ at 30 TeV before(left) and after(right) cuts, see also Item(IV A) for the cut and Table(VI) for the cut flow.

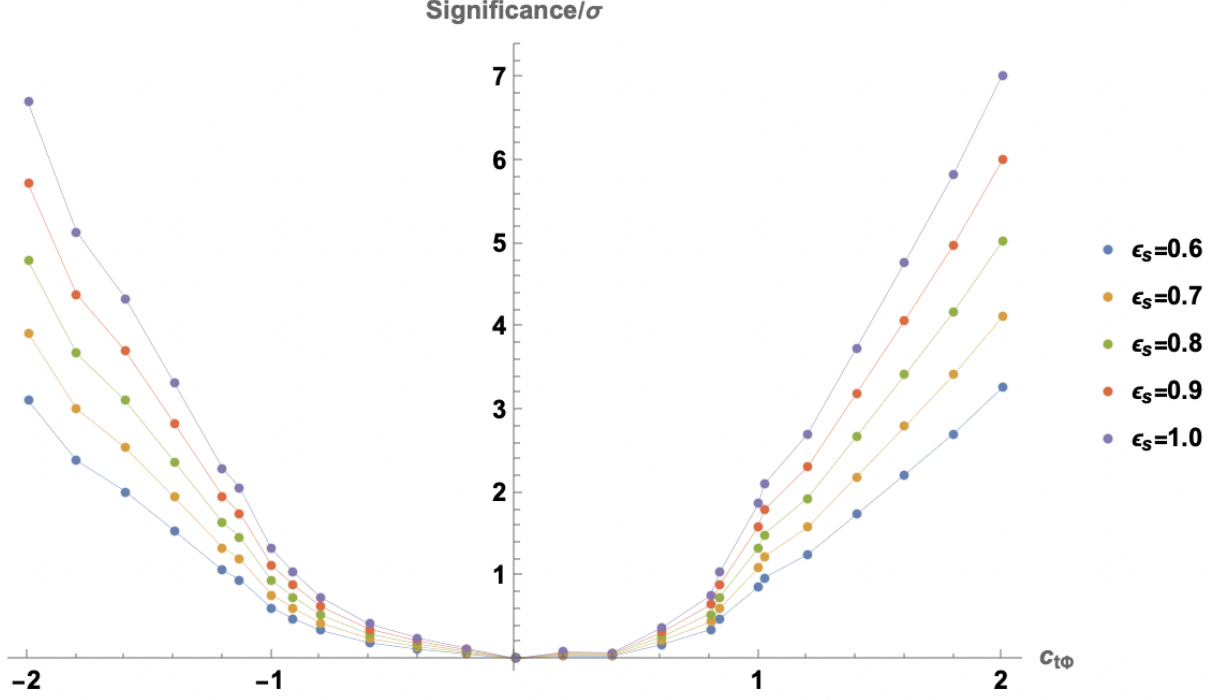


Figure 10. The dependence of statistical significance of the lepton channel of νvtz at 30 TeV on $c_{t\phi}$ (with $\Lambda = 1$ TeV) and spin tagging efficiency ϵ_s , the latter of Z and t/\bar{t} are take to be equal. The b quark tagging efficiency is set to be $\epsilon_b = 0.9$.

B. Semi-lepton Channel

In this subsection we study channel $3l^\pm jj2b + \text{MET}$ with $l = e, \mu$, $b = b/\bar{b}$, which comes from νvtZ through decays: $t \rightarrow bW^+ \xrightarrow{W^+ \rightarrow l^+ \nu_l} bl^+ \nu_l$, $\bar{t} \rightarrow \bar{b}W^- \xrightarrow{W^- \rightarrow jj} \bar{b}jj$ and $Z \rightarrow l^+l^-$, or with $t(l^+) \leftrightarrow \bar{t}(l^-)$.

The main background processes are

$$\begin{aligned}
\mu\mu &\rightarrow \nu\bar{\nu}t_R\bar{t}_R(/t_L\bar{t}_L)Z_L(\text{SM}) \rightarrow 3\nu l^\pm 2bjj \\
\mu\mu &\rightarrow t_R\bar{t}_R(/t_L\bar{t}_L)Z_L \rightarrow 3\nu l^\pm 2bjj \\
\mu\mu &\rightarrow l^+\nu_l W^- Z_L Z_L(/l^-\bar{\nu}_l W^+ Z_L Z_L) \rightarrow \nu 3l^\pm 2bjj \\
\mu\mu &\rightarrow l^+\nu_l W^- Z_L h(/l^-\bar{\nu}_l W^+ Z_L h) \rightarrow \nu 3l^\pm 2bjj \\
\mu\mu &\rightarrow l^+\nu_l W^- hh(/l^-\bar{\nu}_l W^+ hh) \rightarrow \nu 3l^\pm 2bjj
\end{aligned} \tag{26}$$

We will only give the results of 30 TeV, since the limits on δy_t at 10 TeV is too weak ($|C_{t\phi}| < 2 \text{ TeV}^{-1}$).

process	before cuts	cut1	cut2	cut3
BSM($\nu\bar{\nu}ttZ_L$)	229.7×4	228.16×4	218.19×4	213.09×4
SM($\nu\bar{\nu}ttZ_L$)	160.2×4	158.65×4	150.31×4	145.61×4
ttZ_L	2.57×4	2.57×4	2.56×4	2.56×4
$l\nu_l W Z_L Z_L$	20.23×2	20.23×2	1.16×2	1.12×2
$l\nu_l W h Z_L$	124.06×2	124.06×2	124.06×2	0

Table VII: Cut flow of semi-lepton channel of $\nu\bar{\nu}ttz$ at 30 TeV, integrated luminosity is 90 ab^{-1} . The BSM process is simulated at $c_{t\phi} = 2$ (with $\Lambda = 1\text{ TeV}$). Helicity selections are shown in the table. Background processes that have negligible contribution are not listed.

The b tagging efficiency and spin tagging efficiency are set to be $\epsilon_b = \epsilon_s = 1$.

30 TeV

The semi-lepton channel of $\nu\bar{\nu}t_R\bar{t}_R(/t_L\bar{t}_L)Z_L$ has a much larger cross-section than the lepton channel, even though the ratio of the signal cross sections between the semi-lepton and lepton is not as prominent as in $\nu\bar{\nu}t_R\bar{t}_R(/t_L\bar{t}_L)h$, we still expect a higher significance. Moreover, we will perform some cuts to reduce the background and enhance the statistical significance of the processes $\nu\bar{\nu}t_R\bar{t}_R Z_L$ and $\nu\bar{\nu}t_L\bar{t}_L Z_L$. The cuts are listed as below:

- Cut 1: Select $p_T(l) > 40\text{ GeV}$. The purpose of this cut is to reduce the SM part of signal process $\nu\bar{\nu}t_R\bar{t}_R(/t_L\bar{t}_L)Z_L$
- Cut 2: Reject $80\text{ GeV} < M_{b_1 b_2} < 100\text{ GeV}$. The purpose of this cut is to reduce the process $l^+\nu_l W^- Z_L Z_L(/l^-\bar{\nu}_l W^+ Z_L Z_L)$ that have Z decaying to $2b$.
- Cut 3: Reject $120\text{ GeV} < M_{b_1 b_2} < 130\text{ GeV}$. The purpose of this cut is to reduce the process $l^+\nu_l W^- Z_L h(/l^-\bar{\nu}_l W^+ Z_L h)$ that have h decaying to $2b$.

with $b = b/\bar{b}$, $l = l^+l^-$.

The results of the cut flow are summarized in Table(VII), according to which, combined with b tagging efficiency $\epsilon_b = 0.9$ and spin tagging efficiency ϵ_s , we can obtain the corresponding statistical significance Z . Taking $\epsilon_s = 0.9$ and following Eq.(13), we obtain $Z = 7.6(\sigma)$ at $c_{t\phi} = 2$ with $\Lambda = 1\text{ TeV}$. We also show some plots of the events before and after the cuts in Fig.(11). Following the same procedure we can obtain the constraint on $C_{t\phi}$ with

$\epsilon_s = 0.9$ as $-1.18 \text{ TeV}^{-2} \leq C_{t\phi} \leq 1.17 \text{ TeV}^{-2}$ at 2σ and $-0.98 \text{ TeV}^{-2} \leq C_{t\phi} \leq 0.92 \text{ TeV}^{-2}$ at 1σ . Converting them into constraints on δy_t , we get $-7.2\% \leq \delta y_t \leq 7.2\%$ at 2σ and $-5.6\% \leq \delta y_t \leq 6.0\%$ at 1σ .

Statistical significance Z also changes with spin tagging efficiency ϵ_s , as well as with $c_{t\phi}$. The results are summarized in Fig.(12).

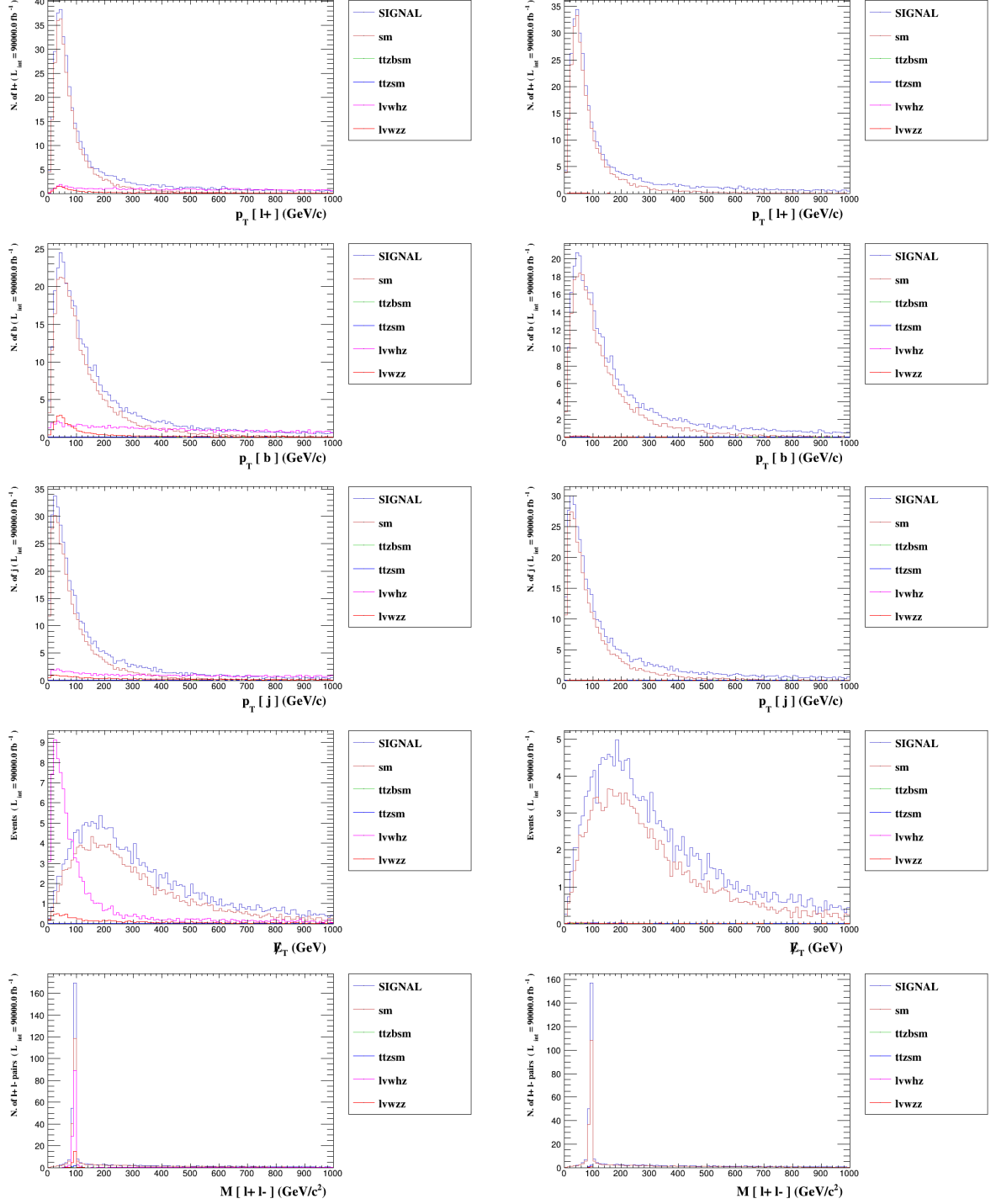


Figure 11. Distributions of the semi-lepton channel of $\nu\bar{t}t\bar{t}Z$ at 30 TeV before(left) and after(right) cuts, see Item(IV B) for the cuts and Table(VII) for event numbers with the cut flow.

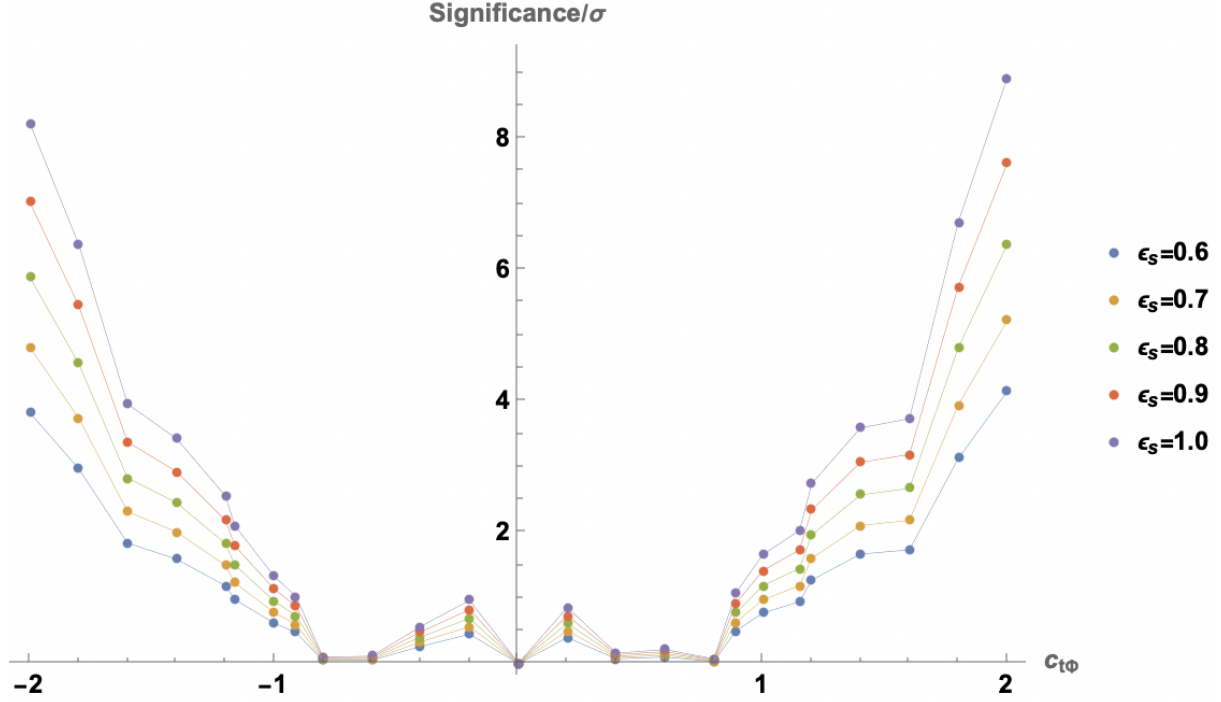


Figure 12. The dependence of statistical significance of the semi-lepton channel of $\nu\nu ttz$ at 30 TeV on $c_{t\phi}$ (with $\Lambda = 1$ TeV) and spin tagging efficiency ϵ_s , the latter of Z and t/\bar{t} are take to be equal. The b quark tagging efficiency is set to be $\epsilon_b = 0.9$.

V. CONCLUSION

In this paper, we studied the measurement of the top Yukawa coupling through $2 \rightarrow 3$ VBS in future muon colliders. We focused on the final states of $\nu\nu tth$ and $\nu\nu ttz$, corresponding to $W^+W^- \rightarrow t\bar{t}h/Z$.

By analysing the related helicity amplitudes and hard processes without decaying, we established the high sensitivity of the processes to the anomalous top Yukawa coupling δy_t . This sensitivity is particularly enhanced by selecting the helicities of $t\bar{t}$ and Z to be $t_R\bar{t}_R/t_L\bar{t}_L$ and Z_L . We also obtain the limits on δy_t for hard processes (Table I) as rough estimations. As can be seen in the table, the limits from $\nu\nu t\bar{t}h$ and $\nu\nu t\bar{t}Z$ are close, with the former better at the positive limits and the latter better at the negative limits. The results from $\nu\nu t\bar{t}h + \nu\nu t\bar{t}Z$ combined are better than both of the two individually. At 30 TeV, it gives the limit on δy_t of $[-0.36\%, 0.92\%]$ at 1σ level.

We then proceed to carry out detailed background analysis of the processes after decaying at 10 TeV (10 ab^{-1}) and 30 TeV (90 ab^{-1}) respectively, with the main focus on the lepton

Channels		E_{cm}	spin tagging efficiency(ϵ_s)	Limits of δy_t	
				1σ	2σ
$\nu t\bar{t}h$	lepton	30 TeV	0.9	[-3.1%, 2.6%]	[-3.2%, 3.4%]
			0.7	[-3.2%, 3.1%]	[-3.7%, 3.8%]
		10 TeV	0.9	[-11.0%, 9.8%]	–
			0.7	[-12.2%, 11.0%]	–
	semi-lepton	30 TeV	0.9	[-1.6%, 1.8%]	[-2.4%, 2.7%]
			0.7	[-2.1%, 2.4%]	[-2.5%, 2.8%]
		10 TeV	0.9	[-7.0%, 6.7%]	[-9.8%, 9.8%]
			0.7	[-8.3%, 7.9%]	[-11.2%, 10.9%]
$\nu t\bar{t}Z$	lepton	30 TeV	0.9	[-5.5%, 5.8%]	[-6.7%, 7.3%]
			0.7	[-5.8%, 6.6%]	[-8.3%, 8.6%]
		10 TeV	–	–	–
	semi-lepton	30 TeV	0.9	[-5.6%, 6.0%]	[-7.2%, 7.2%]
			0.7	[-6.1%, 7.2%]	[-8.3%, 8.6%]
		10 TeV	0.9	–	–

Table VIII: Summary of constraints on δy_t in different channels with different settings. b tagging efficiency is taken to be 0.9 for every analysis. The helicities of $t\bar{t}$ are chosen to be LL/RR , the helicity of Z is chosen to be longitudinal. Spin tagging efficiency of final states are chosen be the same.

and semi-lepton channels. The results are summarized in Table(VIII). For an overall picture, the results from 30 TeV are significantly better than the counter parts from 10 TeV; $\nu t\bar{t}h$ is generally better than $\nu t\bar{t}Z$, but the two are still at the same level; the semi-lepton channels are consistently better than lepton channels, but the differences are smaller than between $\nu t\bar{t}h$ and $\nu t\bar{t}Z$; finally, the variation of the results from changing spin tagging efficiency is minimal. As the most stringent limit on δy_t , at 30 TeV and $\epsilon_s = 0.9$, the semi-lepton channels of $\nu t\bar{t}h$ and $\nu t\bar{t}Z$ constrain δy_t at $[-1.8\%, 1.6\%]$ and $[-5.6\%, 6.0\%]$ at 1σ .

Our results demonstrate promising prospects and importance for $2 \rightarrow 3$ VBS to measure the top Yukawa coupling for futhure muon colliders at 10 TeV and 30 TeV, especially the latter. In particular, the important processes include not only $\nu t\bar{t}h$, but also $\nu t\bar{t}Z$. The

latter process has never been studied before this paper as far as we're concerned. Our analysis (of hard processes) nevertheless show comparable results with those using bin-by-bin analysis. The crucial setting of our approach is to specify the helicities of final states, which dramatically enhanced significance. The spin of a heavy particle has been measured in LHC several times with high precision[30, 31], thus it's reasonable to assume that spin measurement can serve a reliable tool for analysis in future muon colliders. However, further study and improvement is obviously needed, and indeed has potential of bearing great fruit. Finally, we did a comprehensive background analysis with all lepton channels and semi-lepton channels of $\nu t\bar{t}h$ and $\nu t\bar{t}Z$. The best limits on δy_t are worse than hard processes, but the deviations are not very large. It seems that the main factor of the decrease of statistical significance is the smaller event numbers after decaying the heavy particles, not the effects of background processes.

This paper is also limited in several ways. First of all, we only studied $\nu t\bar{t}h/Z$ out of all $2 \rightarrow 3$ VBS processes(Eq.(1)), also didn't include the hadronic channels of $\nu t\bar{t}h/Z$ which have the largest cross sections. Second, our main method in data analysis is still to apply cuts to reduce background, apart from helicity selection. Bin-by-bin analysis, which makes use of the differential cross sections more efficiently, could greatly enhance the constraints on y_t . However, the two methods are not mutually exclusive, it should be possible to combine spin tagging setting with bin-by-bin analysis. This would make the best use of the data and put strongest constraints on top Yukawa. To finally conclude, measuring top Yukawa coupling with $2 \rightarrow 3$ VBS processes has shown great prospects and this paper is only a beginning, it's worth further study and investigation.

ACKNOWLEDGEMENTS

Junmou Chen is supported by NSFC (National Natural Science Foundation of China) no. 12205118.

-
- [1] D.B. Kaplan, H. Georgi and S. Dimopoulos, *Composite higgs scalars*, *Physics Letters B* **136** (1984) 187.

- [2] M.J. Dugan, H. Georgi and D.B. Kaplan, *Anatomy of a composite higgs model*, *Nuclear Physics B* **254** (1985) 299.
- [3] A. Bally, Y. Chung and F. Goertz, *Hierarchy problem and the top Yukawa coupling: An alternative to top partner solutions*, *Phys. Rev. D* **108** (2023) 055008 [2211.17254].
- [4] M. Trodden, *Electroweak baryogenesis*, *Rev. Mod. Phys.* **71** (1999) 1463 [hep-ph/9803479].
- [5] X. Zhang, S.K. Lee, K. Whisnant and B.L. Young, *Phenomenology of a nonstandard top quark Yukawa coupling*, *Phys. Rev. D* **50** (1994) 7042 [hep-ph/9407259].
- [6] H. Baer, V. Barger, J. Dutta, D. Sengupta and K. Zhang, *Top squarks from the landscape at high luminosity LHC*, *Phys. Rev. D* **108** (2023) 075027 [2307.08067].
- [7] ATLAS collaboration, *Search for R-parity violating supersymmetric decays of the top squark to a b-jet and a lepton in $s=13$ TeV pp collisions with the ATLAS detector*, *Phys. Rev. D* **110** (2024) 092004 [2406.18367].
- [8] ATLAS collaboration, *A search for top-squark pair production, in final states containing a top quark, a charm quark and missing transverse momentum, using the 139 fb^{-1} of pp collision data collected by the ATLAS detector*, *JHEP* **07** (2024) 250 [2402.12137].
- [9] ATLAS collaboration, *Probing the CP nature of the top-Higgs Yukawa coupling in $tt^{-}H$ and tH events with $H \rightarrow bb^{-}$ decays using the ATLAS detector at the LHC*, *Phys. Lett. B* **849** (2024) 138469 [2303.05974].
- [10] CMS collaboration, *Measurements of $t\bar{t}H$ Production and the CP Structure of the Yukawa Interaction between the Higgs Boson and Top Quark in the Diphoton Decay Channel*, *Phys. Rev. Lett.* **125** (2020) 061801 [2003.10866].
- [11] CMS collaboration, *Measurement of the top quark Yukawa coupling from $t\bar{t}$ kinematic distributions in the dilepton final state in proton-proton collisions at $\sqrt{s} = 13$ TeV*, *Phys. Rev. D* **102** (2020) 092013 [2009.07123].
- [12] J.P. Delahaye, M. Diemoz, K. Long, B. Mansoulié, N. Pastrone, L. Rivkin et al., *Muon Colliders*, 1901.06150.
- [13] K. Long, D. Lucchesi, M. Palmer, N. Pastrone, D. Schulte and V. Shiltsev, *Muon colliders to expand frontiers of particle physics*, *Nature Phys.* **17** (2021) 289 [2007.15684].
- [14] D. Buttazzo, D. Redigolo, F. Sala and A. Tesi, *Fusing Vectors into Scalars at High Energy Lepton Colliders*, *JHEP* **11** (2018) 144 [1807.04743].

- [15] A. Costantini, F. De Lillo, F. Maltoni, L. Mantani, O. Mattelaer, R. Ruiz et al., *Vector boson fusion at multi-TeV muon colliders*, *JHEP* **09** (2020) 080 [[2005.10289](#)].
- [16] T. Han, D. Liu, I. Low and X. Wang, *Electroweak couplings of the Higgs boson at a multi-TeV muon collider*, *Phys. Rev. D* **103** (2021) 013002 [[2008.12204](#)].
- [17] M. Chiesa, F. Maltoni, L. Mantani, B. Mele, F. Piccinini and X. Zhao, *Measuring the quartic Higgs self-coupling at a multi-TeV muon collider*, *JHEP* **09** (2020) 098 [[2003.13628](#)].
- [18] K. Whisnant, B.-L. Young and X. Zhang, *Unitarity and anomalous top quark Yukawa couplings*, *Phys. Rev. D* **52** (1995) 3115 [[hep-ph/9410369](#)].
- [19] B. Henning, D. Lombardo, M. Rimbau and F. Riva, *Measuring Higgs Couplings without Higgs Bosons*, *Phys. Rev. Lett.* **123** (2019) 181801 [[1812.09299](#)].
- [20] F. Maltoni, L. Mantani and K. Mimasu, *Top-quark electroweak interactions at high energy*, *JHEP* **10** (2019) 004 [[1904.05637](#)].
- [21] M. Chen and D. Liu, *Top Yukawa coupling measurement at the muon collider*, *Phys. Rev. D* **109** (2024) 075020 [[2212.11067](#)].
- [22] Z. Liu, K.-F. Lyu, I. Mahbub and L.-T. Wang, *Top Yukawa coupling determination at high energy muon collider*, *Phys. Rev. D* **109** (2024) 035021 [[2308.06323](#)].
- [23] R.K. Barman et al., *Directly Probing the CP-structure of the Higgs-Top Yukawa at HL-LHC and Future Colliders*, in *Snowmass 2021*, 3, 2022 [[2203.08127](#)].
- [24] M.E. Cassidy, Z. Dong, K. Kong, I.M. Lewis, Y. Zhang and Y.-J. Zheng, *Probing the CP structure of the top quark Yukawa at the future muon collider*, *JHEP* **05** (2024) 176 [[2311.07645](#)].
- [25] A. Dedes, W. Materkowska, M. Paraskevas, J. Rosiek and K. Suxho, *Feynman rules for the Standard Model Effective Field Theory in R_ξ -gauges*, *JHEP* **06** (2017) 143 [[1704.03888](#)].
- [26] J. Chen, C.-T. Lu and Y. Wu, *Measuring Higgs boson self-couplings with $2 \rightarrow 3$ VBS processes*, *JHEP* **10** (2021) 099 [[2105.11500](#)].
- [27] J. Chen, T. Li, C.-T. Lu, Y. Wu and C.-Y. Yao, *Measurement of Higgs boson self-couplings through $2 \rightarrow 3$ vector bosons scattering in future muon colliders*, *Phys. Rev. D* **105** (2022) 053009 [[2112.12507](#)].
- [28] J. Alwall, R. Frederix, S. Frixione, V. Hirschi, F. Maltoni, O. Mattelaer et al., *The automated computation of tree-level and next-to-leading order differential cross sections, and their matching to parton shower simulations*, *JHEP* **07** (2014) 079 [[1405.0301](#)].

- [29] C. Degrande, G. Durieux, F. Maltoni, K. Mimasu, E. Vryonidou and C. Zhang, *Automated one-loop computations in the SMEFT*, [2008.11743](#).
- [30] A. Ballestrero, E. Maina and G. Pelliccioli, *Different polarization definitions in same-sign WW scattering at the LHC*, *Phys. Lett. B* **811** (2020) 135856 [[2007.07133](#)].
- [31] S. De, V. Rentala and W. Shepherd, *Measuring the polarization of boosted, hadronic W bosons with jet substructure observables*, [2008.04318](#).